

**DEVELOPMENT AND *IN VIVO* ANALYSIS OF ANTIGEN-MIMICKING
MONOLAYER-PROTECTED GOLD NANOPARTICLES**

By

Amanda C. Agrawal

Thesis

**Submitted to the Faculty of the
Graduate School of Vanderbilt University
in partial fulfillment of the requirements**

for the degree of

MASTER OF SCIENCE

in

Chemistry

August, 2012

Nashville, TN

Approved:

Professor David E. Cliffl

Professor David W. Wright

TABLE OF CONTENTS

	Page
LIST OF FIGURES.....	iv
Chapter	
I. INTRODUCTION.....	1
A Synthetic Approach to Vaccination.....	1
Biomimetic Gold Nanoparticles.....	2
Tiopronin AuNPs as Scaffolds.....	4
PEG-ylated Tiopronin AuNPs <i>in vivo</i>	6
Glutathione AuNPs <i>in vivo</i>	7
Magic-Sized Monolayer-Protected Clusters as Scaffolds.....	8
II. EXPERIMENTAL.....	9
Reagents.....	9
Synthesis of Tiopronin AuNPs.....	9
Place Exchange of PEG onto Tio AuNPs.....	10
Synthesis of GS AuNPs.....	11
Synthesis of TioEG MPCs.....	12
Synthesis of the Peptide Epitope Mimic of the Protective Antigen of <i>B. Anthracis</i>	12
Place Exchange of PA onto AuNPs.....	13
Nuclear Magnetic Resonance.....	14
Thermogravimetric Analysis.....	14
Transmission Electron Microscopy.....	14
Ion-Mobility Mass Spectrometry.....	15
Animal Models.....	16
ICP-OES Analysis.....	17
Coulter Counter Analysis.....	17
Complete Blood Count.....	18
Histology.....	18
Enzyme-Linked Immunosorbent Assay.....	18
III. RESULTS AND DISCUSSION.....	20
Characterization of AuNPs.....	20
PEG-Tio AuNP Mouse Studies.....	28
GS AuNP Mouse Studies.....	32
TioEG MPC Mouse Studies.....	38
IV. CONCLUSIONS AND FUTURE WORK.....	43
Conclusions.....	43

Future Work	44
Acknowledgements	45
REFERENCES	46

LIST OF FIGURES

Figure	Page
1. X-ray crystal structure of the protective antigen of <i>B. anthracis</i> and illustrations of PA mimics highlighting the conformational and linear epitopes	4
2. Characterization data for Tio AuNPs	21
3. Characterization data for GS AuNPs	24
4. ¹ H NMR spectra of bidentate GS AuNPs functionalized with loop PA or linear PA compared with non-functionalized GS AuNPs	26
5. UV-Vis spectrum of TioEG MPCs compared to inset literature UV-Vis spectrum of Au ₃₆ (SR) ₂₃ magic-sized nanoparticles.....	27
6. ¹ H NMR spectra of TioEG MPCs functionalized with loop PA or linear PA compared with non-functionalized TioEG MPCs.....	28
7. Gold concentration measured using ICP-OES in blood, urine, and organs of mice injected with PEG ₄ -acid-Tio AuNPs and PEG ₄ OH-Tio AuNPs.....	30
8. Coulter Counter analysis of blood from PEG ₄ -acid-Tio AuNP mice and PEG ₄ OH-Tio AuNP mice expressed as a ratio of RBC:WBC counts	31
9. Gold concentration measured using ICP-OES in blood, urine, and organs of mice injected with monodentate GS AuNPs and terminated at 4 and 8 weeks post-exposure.....	34
10. Gold concentration measured using ICP-OES in blood, urine, and organs of mice injected with bidentate GS AuNPs terminated at 8 weeks post-exposure, and blood, urine, and organs of mice inoculated with loop or linear PA functionalized GS AuNPs terminated 4 weeks after injection	36
11. Absorbances measured in ELISA for controls and in sera of mice injected with loop and linear PA-GS AuNPs, GS AuNPs, and saline	37
12. Gold concentration measured using ICP-OES in blood, urine, and organs of mice injected with TioEG MPCs and MPCs conjugated with loop and linear PA.....	39
13. WBC counts obtained by CBC at baseline and 1, 2, 3, and 4 weeks post-exposure in TioEG MPC mice.....	40
14. Calibration curve for control ELISA.....	41
15. Absorbances measured in ELISA for controls and in sera of mice injected with saline, TioEG MPCs, loop and linear PA-TioEG MPCs.....	42

CHAPTER I

INTRODUCTION

A Synthetic Approach to Vaccination

Bacillus anthracis is the rod-shaped, gram positive bacterium responsible for causing the disease anthrax. The anthrax toxin is the major virulence factor and is comprised of three protein precursors: protective antigen (PA), edema factor (EF), and lethal factor (LF).¹ PA and LF combine to form lethal toxin, which carries out intracellular hydrolysis of important host protein substrates. PA and EF combine to form edema toxin, which causes extreme swelling and upsets water homeostasis. Both EF and LF depend on PA for membrane transport and activation, making PA crucial for toxicity and an excellent drug target.

The development of vaccines containing whole pathogens or portions thereof is time-consuming, expensive, potentially hazardous to researchers and patients, and runs the risk of conformational changes that render the drug inactive. An ideal substitute would be produced from media free of pathogen-derived products that can be fully synthesized in a lab and mass-produced. This provides the perfect opportunity to employ biomimetics, or the study of nature for inspiration for designs to solve human problems. In this particular case, the design to be mimicked is PA, so a synthetic peptide epitope mimic of PA conjugated to an appropriate drug delivery vehicle could provide an excellent alternative to the current vaccine. Several types of antigen carriers are already in use, namely large proteins or toxoids such as keyhole limpet hemocyanin (KLH),²

ovalbumin,³ bovine serum albumin,⁴ and tetanus toxoid,⁵ to name a few. However, there are some very concerning drawbacks to these types of carriers. Some incite strong antibody response against themselves, which can overshadow the immune response against the target epitope. Often, only a few conjugation sites on the protein carrier are available for binding to the epitope, so presentation of the peptide is inefficient and antigenic sites on the carrier are sometimes left exposed. Some protein-peptide complexes are unstable and lead to the formation of unusable precipitates. These issues give rise to the need for a different type of scaffold to present synthetic peptide epitopes.

Biomimetic Gold Nanoparticles

An approach to a novel vaccine in the form of a biomimetic gold nanoparticle (AuNP) has been explored in the Wright and Cliffel labs.⁶ Gold is bioinert, and therefore would not elicit an immune response against itself. Nanoparticles can be synthesized to resist precipitation, and are multivalent, or possess the ability to be functionalized with multiple constituents. Nanometer-sized, isolable, thiolate ligand-capped metallic particles were first reported by Brust et al. in 1994.⁷ Since then, AuNPs and monolayer-protected gold clusters (MPCs) have been the subject of much interest because of the simplicity of their synthesis, their stability, and the capability to be repeatedly dried down and redissolved in common solvents without aggregation.⁸⁻¹¹ They display core size-dependent properties, transitioning from metal-like to molecule-like as core size decreases and can be easily characterized by conventional analytical methods.^{8,9} Perhaps most interesting is the ease of functionalization of these particles via well-characterized ligand place-exchange reactions in which free ligands in solution exchange with ligands

bound to the nanoparticle surface to form a mixed-monolayer.^{9,12} Ligands Exchange sites are not static, meaning that thiolates can migrate across the surface of a particle.¹² It is for this reason that AuNPs are such a promising scaffold for attachment of peptide epitope mimics. Cysteine-terminated epitopes can be bound to the nanoparticle surface as monodentate linear peptides or bidentate loops. Migration of the two ends of the loop across the particle surface allows them to position themselves at the proper distance apart for the faithful reconstitution of the epitope's physiological conformation. Surface accessible loops on proteins are common antibody binding sites, and as PA is a loop-rich protein, three peptide epitopes from the C-terminus and two internal loops were synthesized and place-exchanged onto a tiopronin-capped MPC in a previous study by Gerdon et al.⁶ The MPC antigen mimics studied are shown in Figure 1. Binding studies were performed on a quartz-crystal microbalance (QCM) and involved subjecting each type of particle to seven mouse monoclonal anti-PA antibodies. The epitope with the highest binding affinity was found to be PA680B (bidentate), which was preferred over PA680M (monodentate), highlighting the importance of secondary structure in antibody recognition. The development of immunogenic MPCs for *in vivo* studies detailed below utilizes PA680B (loop PA) and PA680M (linear PA).

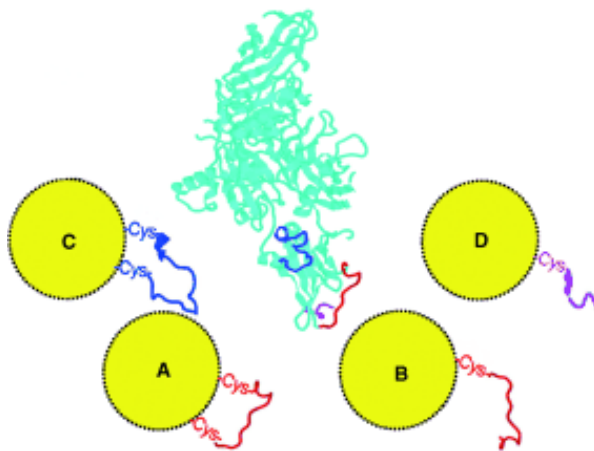


Figure 1. X-ray crystal structure of the protective antigen of *B. anthracis* (middle) and illustrations of PA mimics highlighting the conformational and linear epitopes. Three known epitopes are highlighted in the crystal structure: amino acids 680-692 (red), 703-722 (blue), 730-735 (magenta). Composition of antigen mimics are as follows: A) PA680B-MPC; B) PA680M-MPC; C) PA703B-MPC; D) PA730M-MPC. Reproduced from Reference 6.

Tiopronin AuNPs as Scaffolds

Delivery of therapeutics has been limited by solubility issues, low stability, and rapid clearance from the body.¹³ Tiopronin-capped AuNPs are water-soluble, have high stability, and their circulation half-life can be tuned via PEG-ylation, making Tio AuNPs an excellent candidate for drug delivery agents. If Tio AuNPs are to be used as a scaffold for the PA epitope mimic, it is first necessary to determine the effects of unmodified Tio AuNPs *in vivo*. Opsonization and phagocytosis are the primary biological processes by which foreign particles, including nanoparticles, are removed from the body by the mononuclear phagocytic system (MPS), and are important barriers that must be overcome if nanoparticles are to be used for drug delivery.¹³⁻¹⁶ Opsonin proteins in blood serum quickly bind to the charged surface of nanoparticles, making them easily recognizable by macrophages of the MPS so that they may be removed. Once phagocytes have engulfed the particles, they attempt to degrade it with excretions of enzymes and other oxidative-reactive chemical factors. However, nanoparticles are non-biodegradable, so they are

either removed by the renal system or sequestered in the MPS organs (liver, spleen, bone) if they are above the renal filtration molecular weight threshold of ~100,000 daltons.¹⁴ Oposonized nanoparticles have an increased hydrodynamic diameter, which when large enough will cause substantial damage to organs when the particles attempt to pass through. With sufficient organ damage, death can occur. Choi et al. determined from *in vivo* studies that cadmium selenide quantum dots with a hydrodynamic diameter <5.5 nm underwent rapid urinary excretion, while quantum dots >15 nm were unable to be eliminated.¹⁷ Moghimi et al. note that in rats, polystyrene microspheres >100 nm were physically filtered by the spleen and trapped in the splenic bed.¹⁸ From these size criteria, it would seem as though <5 nm Tio AuNPs may be small enough for successful renal filtration, but previous work in the Cliffel lab showed that Tio AuNPs were not able to escape opsonization because their overall negative charge drew in too many opsonins.¹⁹ The maximum tolerable dose (less severe, non-fatal renal damage) in mice was found to be 200 μ L of 20 μ M (23 mg/kg) Tio AuNPs in sterile saline; morbidity and acute renal failure were seen in all higher concentration groups, along with heavy particle retention in the liver, spleen, and kidneys.¹⁹ The particle was largely cleared from the blood and urine 8 hours post-injection.

In addition to size criteria, Choi et al. and Moghimi et al. also note the importance of surface charge with regard to clearance.^{17,18} Nanoparticles with charged surfaces attract opsonins more than neutral particles, but if the charge is masked or reduced, opsonization can be delayed or even evaded, lengthening circulation time. Polyethylene glycol (PEG) has been shown to eliminate toxicity of nanoparticles by adding protein-resistant properties to the surface to which it is bound.^{13-15,19} When opsonins are attracted

by the charge of the particles, they encounter and compress the longer PEG ligands, forcing them into a denser, higher energy conformation. A repulsive force is created, which balances or overpowers the attractive force of the opsonins, effectively shielding the particle. Longer chain-length PEG is associated with stronger protein repulsion.

PEG-ylated Tiopronin AuNPs in vivo

The Clifffel group has conducted *in vivo* studies in murine models using Tio AuNPs PEG-ylated with a long alkyl chain, alcohol-terminated tetra-EG thiol (MUPEG).¹⁹ MUPEG-Tio AuNPs eliminated morbidity and renal damage, and remained in the bloodstream and urine for the duration of the 4 week study, but still accumulated in the liver, spleen, kidneys, and heart. High concentrations of PEG were shown to produce an immune response as determined by red blood cell (RBC) and white blood cell (WBC) counts, while lower concentrations did not. It was reasoned that anti-PEG antibodies must have been created in response to the sudden high concentration of PEG, which would hinder the particles as a scaffold since the antibody initiates rapid clearance. A carboxylic acid-terminated tetra-EG thiol (PEG₄-acid) and an alcohol-terminated tetra-EG thiol (PEG₄OH)²⁰ were placed exchanged onto Tio AuNPs and studied *in vivo* to determine whether a short chain PEG would be capable of shielding the negative charge of tiopronin from opsonins, and additionally, if the terminus played an important role in circulation time and organ residence. The exchange rate of PEG was controlled so as not to provoke the immune system. However, Armstrong et al. reported that 25% of normal human blood donors have a naturally occurring anti-PEG antibody,²¹ so any vaccine

containing PEG would not benefit this group of people making it necessary to explore other capping ligands that do not require PEG to eliminate toxicity.

Glutathione AuNPs in vivo

Glutathione (GSH) is related structurally to tiopronin, as tiopronin is a glycine derivative while GSH is a tripeptide consisting of L-cysteine, L-glutamic acid, and glycine. Unlike tiopronin which is generated synthetically, GSH is found naturally within the body (0.5-10 mM in animal cells).²² Tiopronin is effectively administered orally for treatment of cystinuria whereas oral administration of glutathione has shown no increase in intracellular glutathione;²³ glutathione is believed to have difficulty crossing the gastrointestinal tract. When administered intravenously, Hahn et al.²⁴ showed by using radiography that free GSH was cleared from the bloodstream within minutes, and examination of the organs showed the greatest accumulation within the renal tissue. It appeared that free GSH was internalized by the organs from the blood within a matter of minutes for biodegradation in the kidney. This was concurred by Wendel et al.²⁵ where free GSH was shown to accumulate in the renal tissue within 20 minutes with a rapid shift to the liver for reassembly. Given the expected organ sequestration of free GSH, a GS AuNP would be likely to provide targeting specification. Additionally, Choi et al. note that zwitterionic or neutral organic coatings on nanoparticles prevent serum protein adsorption,¹⁷ so as a zwitterion, GSH should be able to avoid opsonization without the protection of PEG. After establishing a clearance profile of GS AuNPs, the particles were functionalized with loop and linear PA epitope to attempt to elicit anti-PA antibody production.

Magic-Sized Monolayer-Protected Clusters as Scaffolds

Magic-sized MPCs are highly stable nanoclusters with well-defined structures and numbers of atoms.^{10,26,27} They are atomically monodisperse and many have subnanometer core diameters. There is a fundamental difference between MPCs and their larger AuNP counterparts in the discrete, molecular-like electronic structure and optical properties observed for MPCs. Clusters ranging from ~10 to ~100 atoms exhibit molecular-like HOMO and LUMO electronic features and step-wise optical absorption behavior,²⁸ and distinct electronic features in UV-Vis spectroscopy depending on the core size are observed.²⁹ The major focus of work in the field of magic-sized clusters thus far has been on synthesis, characterization, and the study of their structure and properties rather than on their applications. However, their extreme monodispersity and molecule-like properties make MPCs a promising candidate for use as a scaffold for biomolecule attachment and presentation *in vivo*. TioEG MPCs, magic-sized clusters with a mixed monolayer of tiopronin and tiopronin esterified with ethylene glycol, were studied in mice as is and functionalized with loop and linear PA epitope, as detailed below.

CHAPTER II

EXPERIMENTAL

Reagents

Tetrachloroauric acid trihydrate was synthesized according to the literature³⁰ and stored at -20°C. *N*-(2-Mercaptopropionyl)-glycine (tiopronin, Sigma), glutathione (Sigma), sodium borohydride (Acros Organics), borane-tert-butylamine complex (TBAB, Acros Organics), Thiol-dPEG₄-acid (Quanta Biodesign), α -cyano-4-hydroxycinnamic acid (CHCA, Sigma-Aldrich), Optima nitric acid (Fisher Scientific), hydrochloric acid (EMD Chemicals), trace metal grade nitric acid (Fisher Scientific), trace metal grade hydrochloric acid (Fisher Scientific), methanol (Fisher Scientific), glacial acetic acid (Fisher Scientific), ethylene glycol (Fisher Scientific), deuterium oxide (Cambridge Isotope Laboratories, Inc.), sterile phosphate buffered saline (Mediatech), sterile 0.9% sodium chloride (Hospira, Inc.), ZAP-OGLOBINTM II Lytic Reagent (Beckman Coulter), and Isoton[®] II diluent (Beckman Coulter) were all used as received. A Millipore filtration system (18 M Ω) was used to purify water. 12-mercapto-3,6,9,12-tetraoxadocan-1-ol was synthesized based on a modification of literature methods.³¹

Synthesis of Tiopronin AuNPs

Tiopronin monolayer-protected gold nanoparticles (Tio AuNPs) were created in a 3:1 tiopronin/tetrachloroauric acid trihydrate (HAuCl₄•3H₂O) mole ratio in agreement with a modified Brust reaction.⁸ A mixture of 1 g HAuCl₄•3H₂O (2.54 mmol) and 1.24 g

tiopronin (7.62 mmol) was dissolved in 100 mL 6:1 (v/v) methanol/ acetic acid in a round bottom flask at 0°C. While stirring, 0.95 g (10x mole excess) of NaBH₄ (25.40 mmol) was added quickly. The mixture was allowed to stir for 30 minutes so that the reaction could go to completion. Using a rotary vacuum pump, the solvent was removed and the nanoparticles were dissolved in water. The pH was adjusted to ~1 with concentrated HCl and the crude nanoparticle solution was transferred to cellulose ester dialysis membrane tubing (Thermo Scientific, MWCO 10,000). The tubing was clamped on both ends and floated in 4L deionized water. Dialysis proceeded for 3 days with stirring, with water changes twice daily. The solution was then removed under vacuum and the resulting nanoparticles were characterized.

Place Exchange of PEG onto Tio AuNPs

For the PEG₄-acid experiments, three tiopronin/PEG feed ratios were used. 30 mg Tio AuNP was added to a 1.5 mg (15:1), 10 mg (2:1), or 20 mg (1:1) PEG₄-acid sample in 3 mL of deionized water and allowed to stir for 1 hr. 12-Mercapto-3,6,9,12-tetraoxadocan-1-ol (PEG₄OH) was placed exchanged onto Tio AuNPs using two feed ratios. 4 mg Tio AuNP was added to 0.800 mg (2:1) or 0.107 mg (15:1) PEG₄OH in 2 mL deionized water. Both PEG₄OH reactions were stirred for 30 minutes and all samples were dialyzed as previously described for 3 days. NMR samples were prepared in D₂O and the actual ratios of tiopronin/PEG were determined.

Synthesis of GS AuNPs

Monodentate glutathione (GSH) monolayer-protected gold nanoparticles (GS AuNPs) were synthesized in a 3:1 GSH/HAuCl₄•3H₂O mole ratio in agreement with a modified Brust reaction.⁸ Briefly, 1 g HAuCl₄•3H₂O (2.54 mmol) and 2.34 g GSH (7.62 mmol) were codissolved in 100 mL 6:1 (v/v) methanol/acetic acid in a round bottom flask at 0°C. After 30 minutes of stirring, 0.95 g (10x mole excess with respect to gold) NaBH₄ (25.40 mmol) was added quickly. The solvent was removed under vacuum and the nanoparticle slurry was dissolved in water and filtered through 0.2 micron syringe filters to remove aggregates. The pH of the resulting dark brown nanoparticle solution was adjusted to ~2 with concentrated HCl and the solution was transferred to dialysis membrane tubing (Thermo Scientific, MWCO 10,000). The tubing was clamped on both ends and floated in 4L deionized water. Dialysis proceeded for 3 days with stirring, with water changes twice daily. The solution was then removed under vacuum and the resulting nanoparticles were characterized.

Bidentate GS AuNPs were synthesized in a 1:1 GSH/HAuCl₄•3H₂O mole ratio. Briefly, 1 g HAuCl₄•3H₂O (2.54 mmol) and 0.945 g GSH (2.54 mmol) were codissolved in 100 mL methanol in a round bottom flask at 0°C. Immediately after GSH was dissolved, 0.95 g (10x mole excess with respect to gold) NaBH₄ (25.40 mmol) was added quickly and the solution was allowed to stir for 30 minutes. MeOH was removed via centrifugation, and the particles were washed with MeOH and centrifuged 3x. After the final decantation the particles were dissolved in water and the solution was transferred to dialysis membrane tubing (Thermo Scientific, MWCO 10,000). The tubing was clamped on both ends and floated in 4L deionized water. Dialysis proceeded for 3 days with

stirring, with water changes twice daily. The solution was then removed under vacuum and the resulting nanoparticles were characterized.

Synthesis of TioEG MPCs

Monolayer-protected gold clusters passivated with tiopronin/tiopronin esterified with ethylene glycol (TioEG MPCs) were synthesized in a 3:1 tiopronin/HAuCl₄•3H₂O ratio by adding 0.5037 g HAuCl₄•3H₂O (1.28 mmol) and 0.6367 g tiopronin (3.90 mmol) to 40 mL ethylene glycol heated to 70°C. The reaction was stirred for about 7 minutes and reduced with 1.1005 g TBAB (12.7 mmol, 10x mole excess) in 10 mL ethylene glycol heated to 55°C. Stirring proceeded for 1 hr at 70°C upon which the reaction was removed from heat and etched with HCl for 4 days at room temperature. Excess ethylene glycol and tiopronin were removed via dialysis for 7 days and the nanoparticles were dried down for characterization.

Synthesis of the Peptide Epitope Mimic of the Protective Antigen of B. Anthracis

The epitope mimic of the protective antigen (PA) of *B. anthracis* was synthesized using standard continuous-flow Fmoc solid-phase peptide synthesis methods. The PA loop is a 15-mer peptide of the sequence CKYNDKLPLYISNPC. Linear PA was also synthesized by omitting one cysteine, giving the sequence KYNDKLPLYISNPC. Resin (200 mg) was weighed out and soaked for 30 minutes in dimethylformamide (DMF). Each amino acid coupling cycle was carried out in six-fold excess with respect to moles of resin using 1:1:1:2 amino acid/HBTU/HOBt/DIEA in DMF for 1 hour. Before each new cycle, the resin was washed 3x in DMF, 3x in methanol, and 3x in DMF.

Deprotection, or removal of the Fmoc groups, was achieved through treating the resin with 20% piperidine in DMF for 30 minutes and again rinsing three times each with DMF, methanol, and again with DMF. After the last coupling cycle, the peptidyl resin was deprotected and rinsed as before with an additional rinsing of DCM three times. The resin was then incubated for 30 minutes in 50% acetic anhydride in DCM to acylate the N-terminal amines before being rinsed three times with methanol and dried with vacuum filtration. A 4 mL trifluoroacetic acid (TFA) solution was made with 90% TFA, 5% Thioanosole, 3% Anisole, and 2% ethanedithiol (EDT). The resin was exposed to the TFA solution for 1 hour to cleave the peptides from the resin, filtered through glass wool, and the peptides were added to chilled ether. The peptides were purified using reversed-phase HPLC, frozen in ether, and lyophilized.

Place Exchange of PA onto AuNPs

For a ligand to peptide feed ratio (L/P) of 25:1 GS/PA, 20 mg GS AuNP was added to 1.63 mg loop PA or 1.54 mg linear PA in 6.66 mL deionized water and stirred for 3 days at room temperature. For 25:1 TioEG/PA, 25 mg TioEG MPC was added to 3.94 mg loop PA or 3.72 mg linear PA in 25 mL deionized H₂O at room temperature. All reactions were purified by dialysis for 3-5 days and actual ratios were determined by NMR.

Nuclear Magnetic Resonance

^1H NMR spectra for concentrated samples of free ligand and nanoparticles dissolved in deuterium oxide were collected on a Bruker AV-400 instrument operating at 400 MHz.

Thermogravimetric Analysis

An Instrument Specialist TGA-1000 was used to measure the weight change of a ~4.5 mg sample of nanoparticles in a platinum pan as a function of temperature to determine the percent by mass organic composition of the particles. Nitrogen flow was set to 60 mL min^{-1} and the temperature was ramped from 25-100°C at a rate of 15°C/min, 100-110°C at a rate of 1°C/min, and then 110-800°C/min at a rate of 20°C/min.

Transmission Electron Microscopy

A dilute solution of nanoparticles dissolved in 1 mM HCl or deionized H_2O was dropped onto a 400 mesh copper grid coated with an ultrathin holey carbon film purchased from Ted Pella, Inc. and allowed to dry by slow evaporation. Images of the TEM grid were obtained at a magnification of 150,000× using a Philips CM20 instrument operating at 200 keV. The diameters of >100 particles were measured in nanometers from the negatives using ImageJ software (NIH, <http://rsb.info.nih.gov/ij/>) and used to determine an average core diameter of the nanoparticles.

Ion-Mobility Mass Spectrometry

In accordance with previous experiments,³² nanoparticle samples were dissolved in 10 μL deionized H_2O and combined with 100 μL saturated CHCA and 1% NaCl in MeOH or up to 1:1 $\text{H}_2\text{O}/\text{MeOH}$ depending on AuNP solubility. A 1 μL portion of each was deposited on a stainless steel plate using the dried droplet method.³³ All MALDI-IM-MS analyses were performed using a Synapt HDMS (Waters Corp., Manchester, UK) operating in positive ion mode, equipped with a frequency-tripled Nd:YAG (355 nm) laser operated at a pulse repetition frequency of 1000 Hz. Gold-containing ion signals were extracted and identified using the MassLynx 4.1 (Waters Corp.) software package. 0.5% relative abundance and 15 ppm mass accuracy cutoffs were used to reduce false positive identifications, and the monoisotopic ion abundances for the identified peaks were normalized to the expected monoisotopic abundance for each respective ion. The final set of identified peaks was used in quantitation calculations by the application of eq 1:

$$\left(\frac{X}{X+Y}\right)_{\text{AuNP}} = \frac{\sum C_{X,Y}(X)}{\sum C_{X,Y}(X+Y)} \quad (1)$$

For a nanoparticle with a binary ligand mixture, X and Y, the term on the left denotes the mole fraction of ligand X on the entire nanoparticle. On the right, the numerator is the sum of the multiples of the ion count ($C_{X,Y}$) and the number of X ligands present in each respective peak. The denominator is the sum of the multiples of the ion count ($C_{X,Y}$) and the total number of ligands (X þ Y) present in each respective peak. Together, these represent a mole fraction of the ligand X present on the nanoparticles.

Animal Models

Animals were female, 16-17 week old BALB/cAnNHsd mice weighing 20-22g and purchased from Harlan Sprague Dawley, Inc. The mice were housed under the supervision of full-time veterinarians and staff in a Vanderbilt Division of Animal Care (DAC) facility which was fully certified by the Association for the Assessment and Accreditation of Laboratory Animal Care (AAALAC). Animals were given *ad libitum* access to food and water and the animal room had a controlled photoperiod of 12 hr on, 12 hr off. All procedures were carried out in accordance with an Institutional Animal Care and Use Committees (IACUC) approved protocol. Mice were allowed one week to acclimate to their new housing prior to experimentation. Nanoparticles were dissolved in phosphate buffered saline (PBS) or sterile saline and injected subcutaneously. The two dosage concentrations used were 20 mg/kg (3 mg dissolved in 1.5 mL PBS) and 80 mg/kg (12 mg dissolved in 1.5 mL PBS). Each mouse was injected with a total volume of 200 μ L nanoparticle solution. Baseline blood and urine samples were collected 1 week prior to injection (0 week) and at specific time points post-injection. Blood was drawn via submandibular bleeding³⁴ according to NIH bleeding guidelines for mL blood per kg body weight that can safely be taken per 2 weeks.³⁵ Urine was collected on cellophane sheets while avoiding fecal contamination as described in the literature.³⁶ Blood and urine were analyzed for gold content via inductively coupled plasma optical emission spectroscopy (ICP-OES) and red and white blood cell counts were determined by Coulter Counter or complete blood cell count to monitor immune response. The mice were euthanized 4 or 8 weeks post-injection via CO₂ asphyxiation and organs were harvested for histology and trace metal analysis.

ICP-OES Analysis

Samples were prepared as previously described¹⁹ with modifications. For mice injected with PEG-Tio AuNPs, blood and urine samples were prepared by diluting 5 μ L of the fluid in 1 mL aqua regia (3:1 hydrochloric acid/ nitric acid,). The blood samples were digested 24 hr in aqua regia before being further diluted in 9 mL 2% nitric acid (Optima grade, Fisher Scientific) while the 2% nitric acid was immediately added to the urine samples which required no digestion time. Organs were weighed and dissolved in concentrated nitric acid for 48 h and heated to dryness. The organ residues were then reconstituted in 1 mL aqua regia where they were allowed to digest a further 24 h, and diluted in 9 mL 2% nitric acid. Blood and organ samples were centrifuged and decanted to remove remaining tissue and cells. The values obtained for the organs were adjusted for weight and presented as concentration per gram organ. For mice injected with GS AuNPs and TioEG MPCs, trace metal grade nitric and hydrochloric acids were used to make aqua regia. Biological samples were diluted with 10% aqua regia in water. Measurements were made on a Perkin-Elmer ICP-OES Optima 700 DV using a Burgener Peek Mira Mist[®] nebulizer with an argon plasma flow of 15 L min⁻¹, nebulizer flow of 0.65 L min⁻¹, auxiliary flow of 0.2 L min⁻¹, pump flow of 1.6 mL min⁻¹, RF power at 1450 W, and a delay time of 30 s. Spectra were collected at a wavelength of 267.595 nm in triplicate and averaged.

Coulter Counter Analysis

Blood was analyzed on a Beckman Z1 Coulter Particle Counter. Samples were prepared for cell count analysis by diluting 40 μ L whole blood in 20 mL Isoton[®] II

Diluent (Beckman Coulter) for a 1:500 dilution of the blood specimen to be used as the WBC solution. The RBC solution was made by pipetting 200 μ L of the WBC solution into 19.8 mL diluent to obtain a 1:50,000 dilution. The WBC solution received 8-10 drops of ZAP-OGLOBINTM II lytic reagent (Beckman Coulter) and was agitated slowly. Red and white blood cell counts were then collected in triplicate and averaged.

Complete Blood Count

Blood was submitted to the Vanderbilt Comparative Pathology & Research Histology, Translational Pathology Shared Resource for complete blood count (CBC). 20 μ L of whole blood samples were analyzed on a FORCYTETM Veterinary Hematology Analyzer manufactured by Oxford Science Inc.

Histology

Organs were excised shortly after euthanasia and sections of kidney were immediately fixed in 10% formalin, neutral buffered with 0.03% eosin (Sigma-Aldrich), and sent to Vanderbilt University Medical Center Immunohistochemistry Core Lab for hematoxylin and eosin (H&E) staining. The slides were interpreted by K. Salleng, D.V.M., Vanderbilt University Division of Animal Care.

Enzyme-Linked Immunosorbent Assay

Materials from the Anthrax Protective Antigen 83 ELISA Kit Cat. No. 800-100-P83 from Alpha Diagnostic were used for all assays. To each capture antibody-coated well, 300 μ L wash solution was added and the well plate was left to stand for 5 minutes.

The wash solution was dumped and 100 μL of 200 ng/mL PA standard was added to each sample well. 100 μL wash solution was added to the blank wells. After incubation on a plate shaker for 2 hr, the solution was dumped and the wells were washed 5x with 200 μL wash solution. In the wells used in the calibration curve, 100 μL 1:100 diluted anti-PA83 HRP conjugate from the kit was mixed with 0, 10, 25, 50, 75, 90, or 100 μL 1:100 diluted unlabeled anti-PA83 antibody 110 (Cat. No. C86110M, Meridian Life Science). In the serum wells, 100 μL HRP antibody was mixed with 100 μL 1:20 diluted serum in the GS AuNP studies or 50 μL undiluted serum in the TioEG MPC studies, from mice injected with saline, nanoparticle, nanoparticle functionalized with loop PA, and nanoparticle functionalized with linear PA. Blank wells again received 100 μL wash solution. The plate was again incubated for 2 hr, dumped, and washed 5x with wash solution. To activate the fluorescently labeled HRP antibodies, 100 μL TMB substrate was added to all wells and allowed to develop in a dark drawer for up to 15 min. Once wells had developed a blue color, 100 μL Stop Solution (1% sulfuric acid) was added to all wells, turning them yellow. The absorbance was measured immediately afterwards at 450 nm.

CHAPTER III

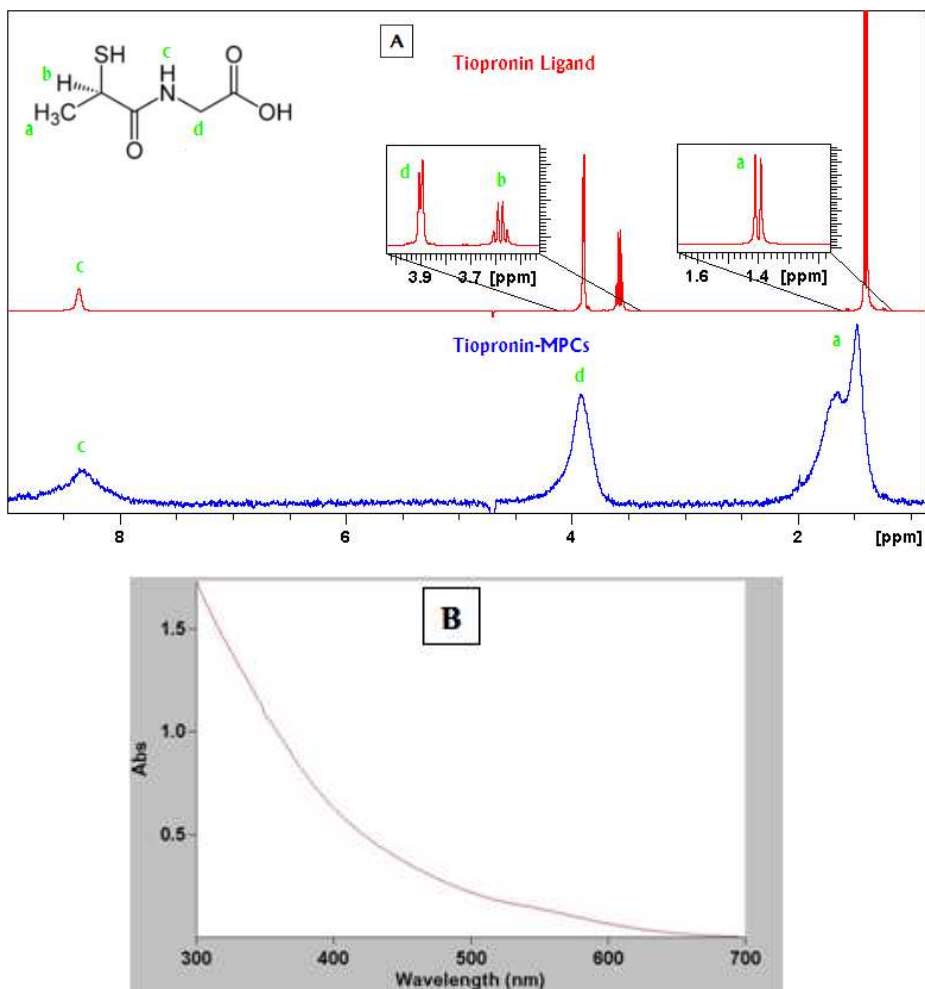
RESULTS AND DISCUSSION

Characterization of AuNPs

Nanoparticles were characterized using analysis methods documented in the literature:⁸ NMR, UV-Vis, TGA, and TEM. In the NMR spectra of free ligands, the peaks are sharp and well-defined because the chemical environment of each ligand is identical. Once bound to the nanoparticle surface, the chemical environment of each ligand is slightly different with respect to the movement and positions of the surrounding bound ligands. Broadening of the peaks in the NMR spectra of nanoparticles is observed because the signals from these varying states are superimposed and overlap. Additionally, the broadened peaks of AuNP NMR spectra are characteristic of nanoparticles because the rotational motions of the larger object (AuNP vs. free ligand) are slower, allowing for longer relaxation times (T_2 spin-spin relaxation) and thus broader peaks.^{8,37} The gold core absorbs strongly in the UV region, with rapid decay of absorption into the visible. A broad surface plasmon (SP) band occurs around 520 nm in the spectra of solutions containing AuNPs that increases in intensity with increasing average core diameters.⁹ The absence of a SP band is characteristic of very small particles with diameters less than ~5 nm. TGA analysis allows for the rough determination of percent organic and percent gold composition of the nanoparticle sample. Mass is plotted vs. temperature, so as temperature increases, mass decreases. After the initial water loss step, organic matter is lost leaving behind the gold core. TEM

analysis reveals the average core size of the nanoparticle samples. Characterization data is shown below.

In Figure 2A, the protons that correspond to each peak are labeled in green on the structure of tiopronin. There is no peak for the thiol proton because it exchanges with deuterium in the polar H₂O/D₂O solution. This peak appears when a less polar solvent system is used, such as CDCl₃/DMSO-d₆. The carboxylic acid proton peak is absent for similar reasons. The amine peak occurs at 8.3 ppm, methylene at 3.9 ppm, methine at 3.6 ppm, and methyl at 1.4 ppm. Methine does not appear in the Tio AuNP spectrum because it is too close to the gold surface when tiopronin is bound to the nanoparticles.



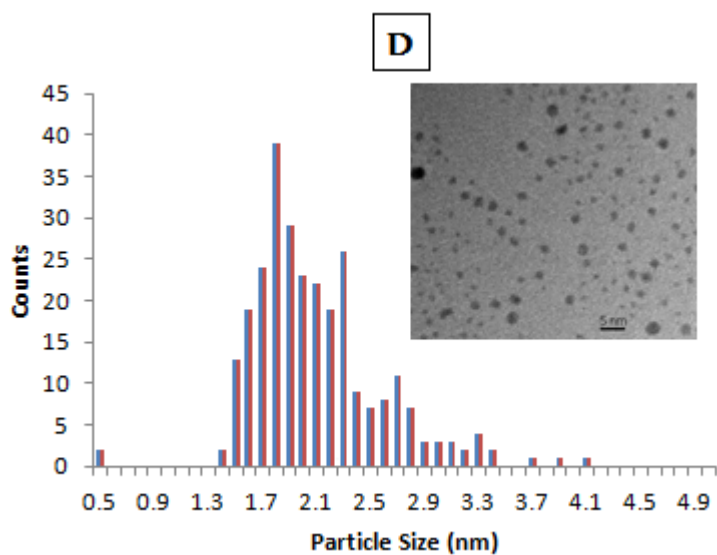
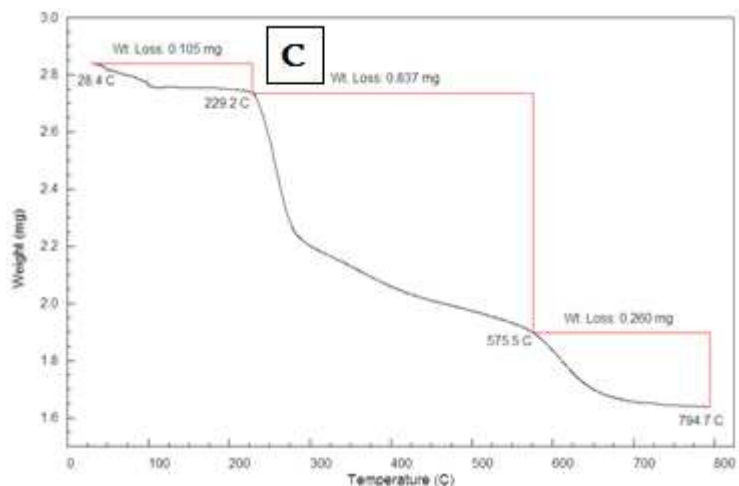
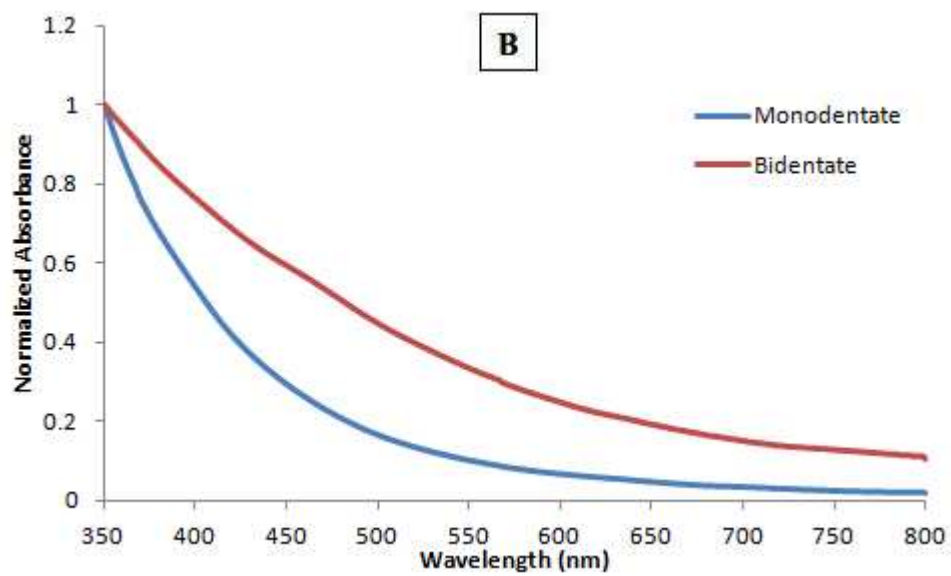
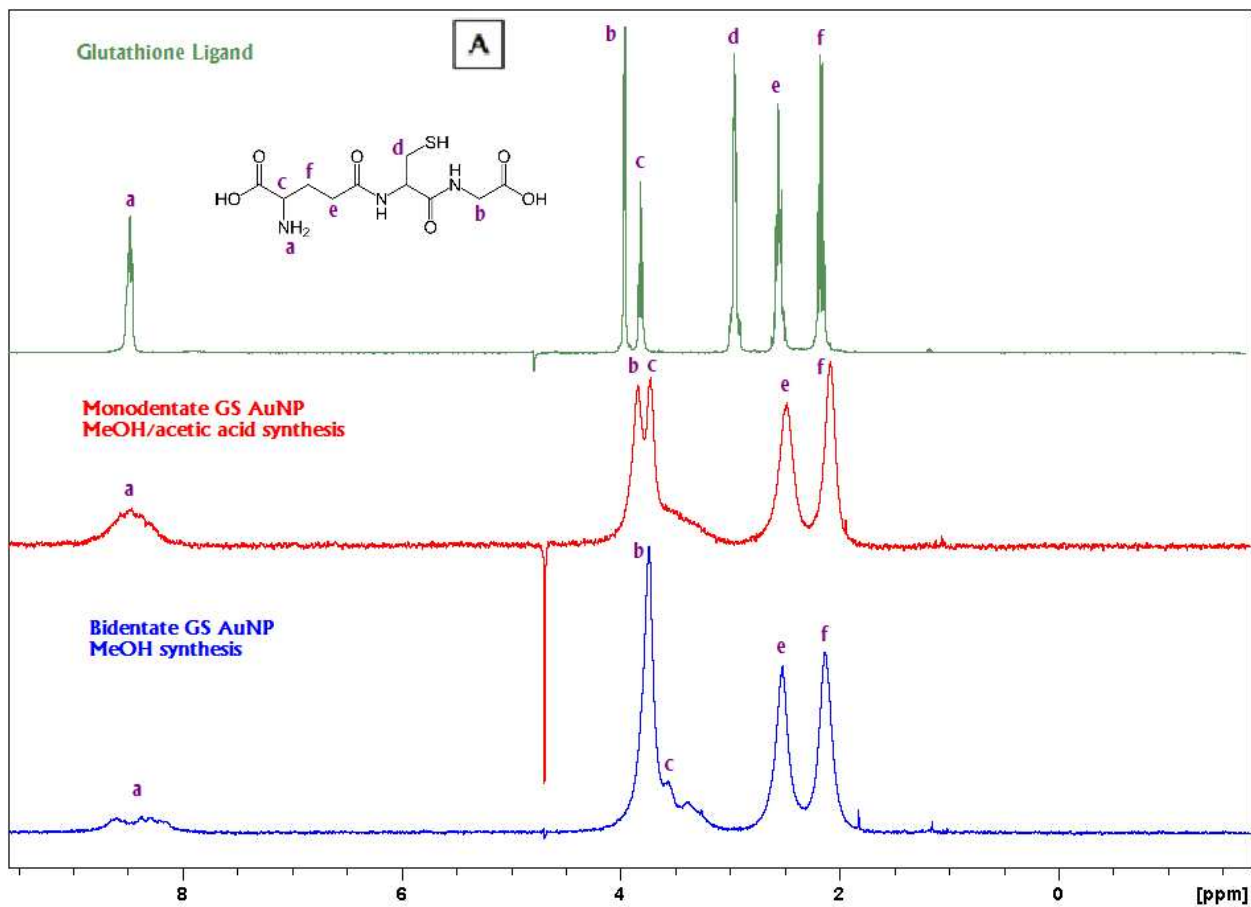


Figure 2. Characterization data for TiO_2 AuNPs. A) ^1H NMR spectrum of tiopronin ligand (red) and characteristically broadened TiO_2 AuNP spectrum (blue); B) slight bump at ~ 520 nm in the UV-Vis spectrum indicates the presence of a small percentage of clusters or aggregates greater than 5 nm in diameter; C) TGA shows initial water loss step, then two organic losses, accounting for 40% of the particle mass; D) histogram displaying particle size distribution and representative TEM image showing an average particle diameter of 2.1 ± 0.5 nm.

Characterization data for monodentate and bidentate GS AuNPs are shown in Figure 3. The peaks corresponding to the labeled protons in the glutathione structure are labeled in the ^1H NMR spectra of GSH (green), and in monodentate (red) and bidentate GS AuNPs (blue). At 8.2 ppm, the amide peak occurs and is present in all three spectra. Peaks b, d, e, and f correspond to methylenes while c is due to methine. The signal of the

methylene closest to the thiol, peak d, is quenched in the AuNP spectra because of the proximity to the gold surface. The dissimilarity in magnitude of peaks b and c between monodentate and bidentate GS AuNPs is due to a variety of molecule orientations on the particle surface and differing packing densities. In monodentate GS AuNPs, GSH is attached to the gold surface by a gold-sulfur bond, while in bidentate GS AuNPs, some GSH ligands are not only attached through the sulfur bond, but also through a gold-nitrogen bond. This is further evidenced in the depression of peak a in the NMR spectrum of bidentate GS AuNPs. Another discrepancy between the particles born of the two syntheses can be found in TGA analysis. Monodentate GS AuNPs were determined to be 59% organic, while bidentate GS AuNPs were only 47% organic. This may be explained by the fact that more ligand was available in the monodentate synthesis where a 3:1 ligand/gold ratio was employed compared to the 1:1 ratio used in the bidentate synthesis. The higher availability of GSH and perhaps the differing solvent systems allowed for more GSH to attach to the surface of monodentate nanoparticles. Despite the differences in the protecting layers, the average core sizes for the two batches were very similar, with 2.7 ± 0.7 nm for monodentate and 2.7 ± 0.6 nm for bidentate GS AuNPs.



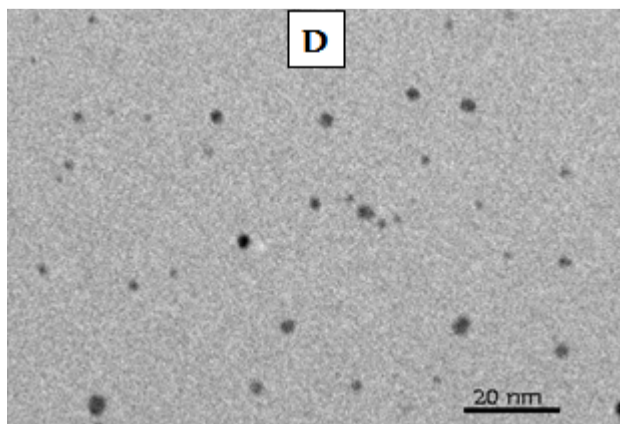
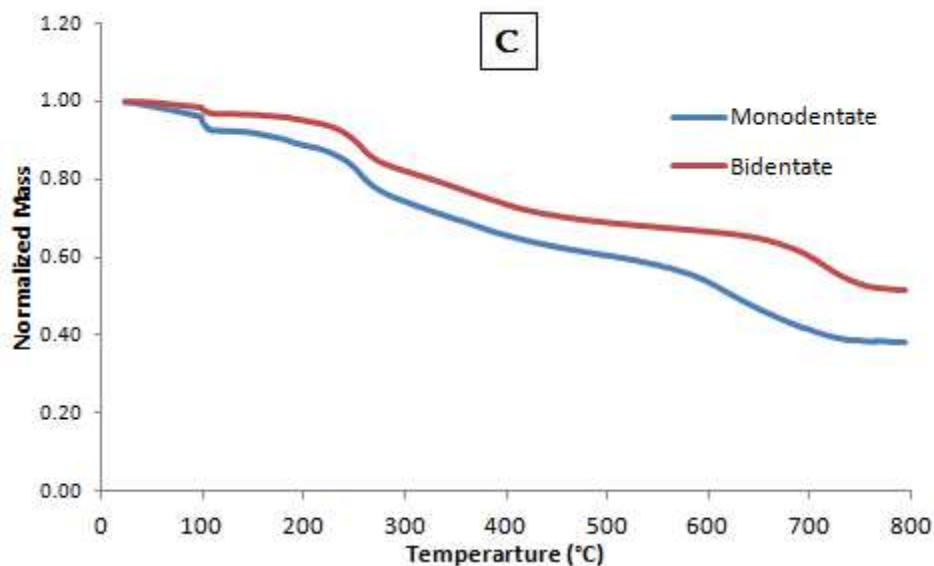


Figure 3. Characterization data for GS AuNPs. A) ^1H NMR spectra of GSH ligand (green), and monodentate GS AuNPs (red), and bidentate GS AuNPs (blue) showing characteristic peak broadening of nanoparticles; B) absence of a SP band at 520 nm in the UV-Vis spectrum indicates particles smaller than 5 nm in diameter; C) after subtracting water loss in the first weight loss step, the organic loss in the second step in TGA analysis accounts for 59% of the total mass in monodentate GS AuNPs, and 47% in bidentate GS AuNPs 2; D) representative TEM image showing an average particle diameter of 2.7 ± 0.7 nm.

Using NMR quantification, the ratio of ligand to peptide (L/P) on the nanoparticle surface was determined. The two peaks at 2.2 and 2.5 correspond to 4 methylene protons in glutathione, and the small peak around 0.8 ppm is from the 18 methyl protons from leucine and isoleucine in PA. In each spectrum, both of these peaks were integrated and the PA peak was calibrated to 18. The area of the two glutathione peaks was divided by

4 and the PA peak was divided by 18 to give an actual L/P. For loop PA-GS AuNPs, the ratio was found to be 32:1 GS/PA, while for linear PA-GS AuNPs, the ratio was 40:1 GS/PA.

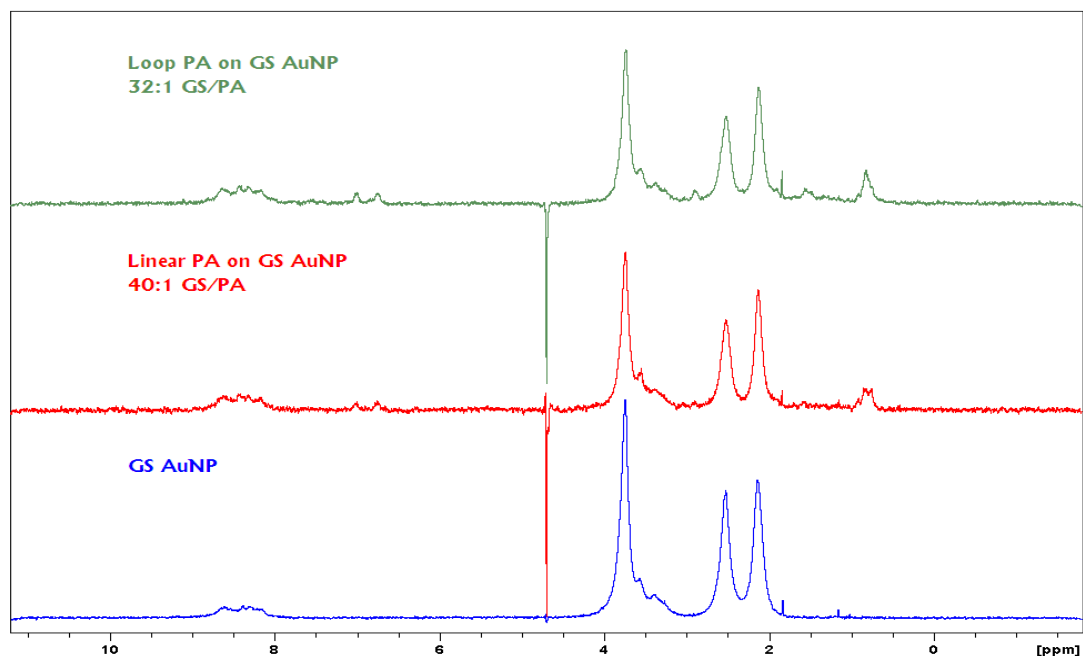


Figure 4. ^1H NMR spectra of bidentate GS AuNPs functionalized with loop PA (green) or linear PA (red) compared with non-functionalized GS AuNPs (blue). NMR quantification yielded a 32:1 L/P ratio for loop PA and a 40:1 L/P ratio for linear PA.

TioEG MPCs were characterized by UV-Vis, IM-MS, NMR, and TEM. The TEM images (not shown) revealed particles that were so small that the resolution of the instrument was not high enough to obtain an average core diameter. However, by comparing the UV-Vis spectrum to one published by Nimmala et al.,³⁸ it was deduced that the TioEG MPCs were most likely of the formula $\text{Au}_{36}(\text{SR})_{23}$. Rather than exhibiting the surface plasmon band present around 520 nm in larger gold nanomaterials (>5 nm) particles <2 nm in size display distinct electronic features in the UV-Vis spectrum.³⁹ IM-

MS analysis suggested that approximately 50% of the tiopronin ligands on the particle surface were esterified with EG.

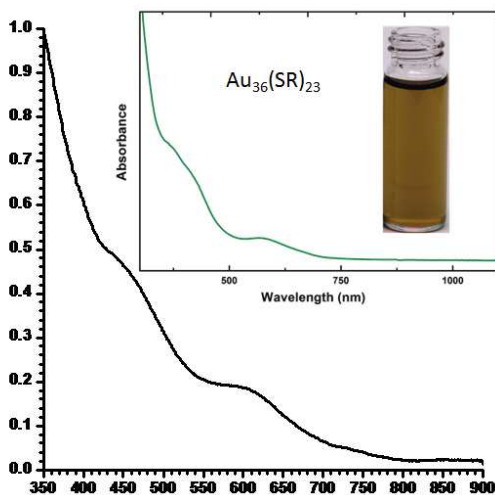


Figure 5. UV-Vis spectrum of TioEG MPCs compared to inset literature UV-Vis spectrum of Au₃₆(SR)₂₃ magic-sized nanoparticles. Inset reproduced from Reference 38.

The L/P was determined using the same method described for quantifying GS AuNPs, using the large peak around 1.5 ppm corresponding to the three methyl protons in tiopronin. The ratio of TioEG/PA for loop PA was found to be 29:1, and 26:1 for linear PA.

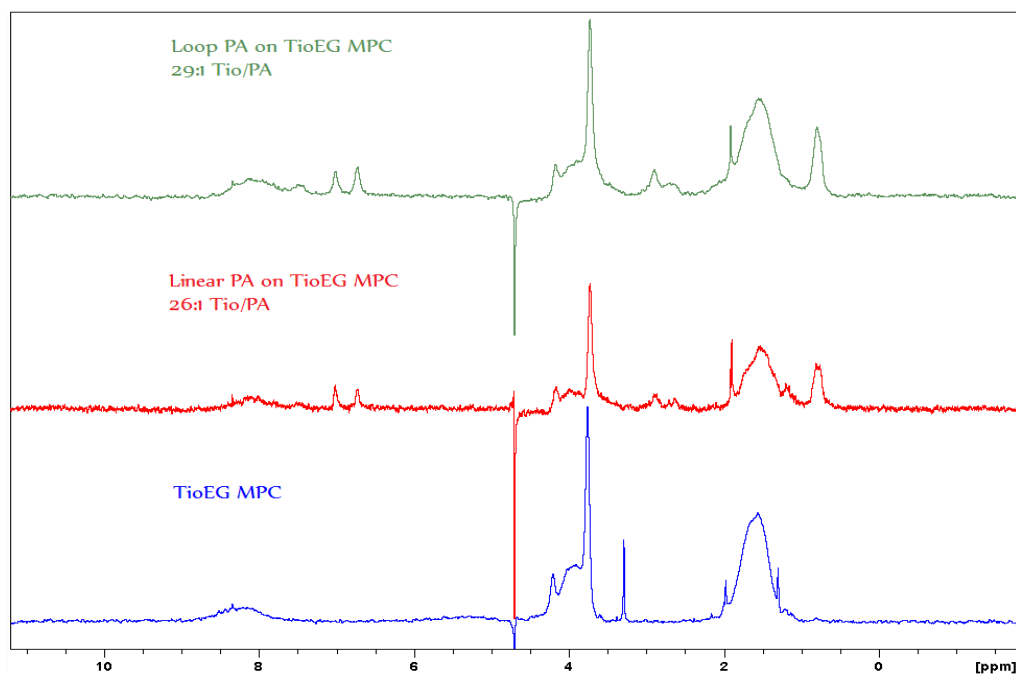


Figure 6. ¹H NMR spectra of TioEG MPCs functionalized with loop PA (green) or linear PA (red) compared with non-functionalized TioEG MPCs (blue). NMR quantification yielded a 29:1 L/P ratio for loop PA and a 26:1 L/P ratio for linear PA.

PEG-Tio AuNP Mouse Studies

ICP-OES analyses for gold concentration in blood, urine, and organ samples from mice injected with PEG₄OH-Tio AuNPs or PEG₄-acid-Tio AuNPs are shown below in Figure 7. Both types of particles showed a low concentration in the blood and a high concentration in the urine in the first 24 hours after injection. At the 2 and 4 week collections of blood and urine, the particle concentration was negligible. Since the majority of both particle types cleared within 24 hours, compared to the previously studied MUPEG-Tio AuNPs¹⁹ which had an alcohol terminus and a clearance time of >4 weeks, it is likely that the chain length rather than the terminus affects circulation time. Organ analysis revealed a repeat in the trend seen in MUPEG-Tio mixed monolayer nanoparticles versus Tio AuNPs:¹⁹ while Tio AuNPs accumulated in high concentrations in all the organs in question, the PEG-Tio AuNPs had lower concentrations. In general,

the more PEG exchanged onto the particle, the lower the concentration in the organs, the exception being the livers of PEG₄-acid-Tio AuNP mice where the reverse trend was observed. This implies tunability in organ targeting by adjusting the exchange rate. Long chain MUPEG-Tio AuNPs accumulated in the organs and blood in higher concentrations than the short chain PEG-Tio AuNPs, but had a lower concentration in the urine as it wasn't being cleared as effectively. Therefore shorter PEG ligands afford shorter clearance time and less organ retention. A possible explanation of why particles coated with smaller amounts of PEG accumulate in the organs at a higher rate is that incomplete surface coverage with PEG left charged areas on the nanoparticle surface unguarded against opsonins, making the particles more likely to be sequestered in the MPS organs than filtered through the renal system because of their increased hydrodynamic diameter.

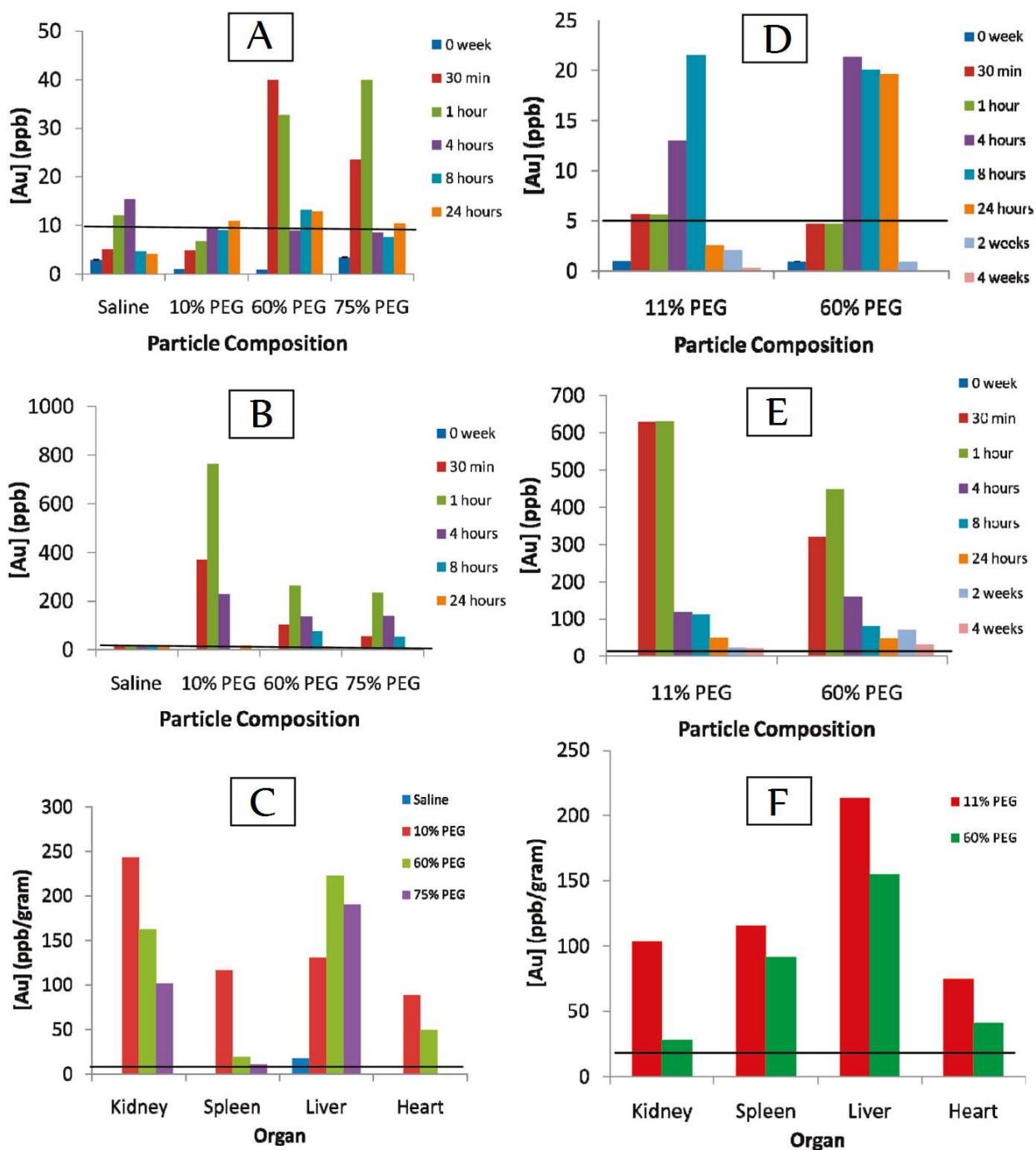


Figure 7. Gold concentration measured using ICP-OES in A) blood, B) urine, and C) organs of mice injected with PEG₄-acid-Tio AuNPs, and in D) blood, E) urine, and F) organs of mice injected with PEG₄OH-Tio AuNPs. Samples contained 5 μ L biological fluid or whole organ dissolved in 10 mL 10% aqua regia. The 2 and 4 week time-points for blood and urine are not shown for the PEG₄-acid studies because the measurements were virtually 0 ppb. Both particle compositions were essentially cleared from the blood and urine within 24 hours and were retained in the organs. Figure modified from Reference 20.

A graphical representation of the blood cell count expressed as the ratio of red blood cells (RBC) to white blood cells (WBC) at 0, 2, and 4 weeks post-injection with PEG-Tio AuNPs is shown in Figure 8. MUPEG caused an increase in WBC count at high concentrations,¹⁹ correlating immune response to PEG concentration. There is no statistically significant change in the RBC:WBC ratio over the four week period for the saline group or lowest percent exchange PEG₄-acid, indicating no immune response. At 60% and 75% PEG₄-acid, there is an increase in RBC count at 4 weeks which causes a significant change in the RBC:WBC ratio (asterisked, $p < 0.01$). This does not signify an immune response as there was no significant change in WBC count. No immune response was invoked by the particles at either percent PEG₄OH coverage. These results suggest that ~10% PEG coverage is sufficient to alleviate nanotoxicity without eliciting an immune response.²⁰

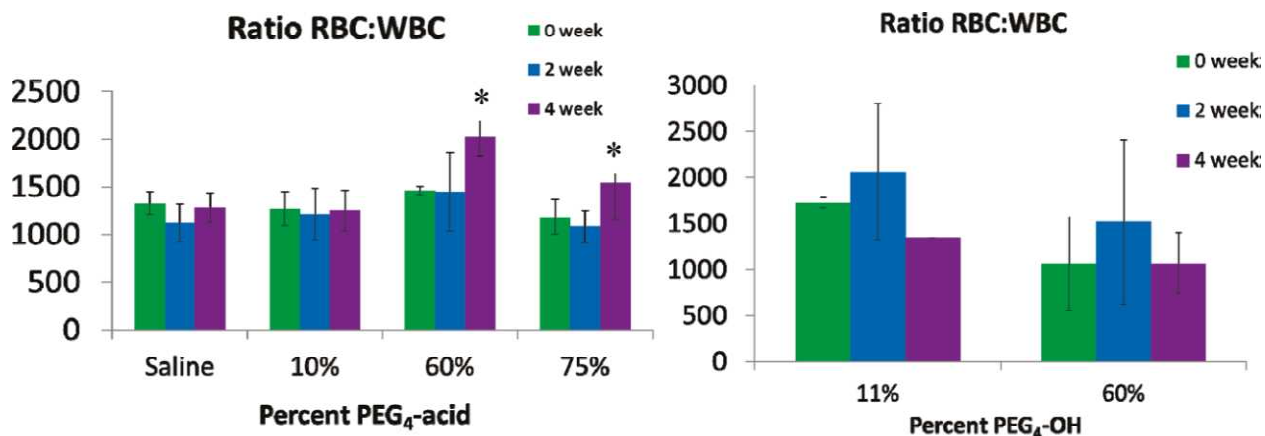


Figure 8. Coulter Counter analysis of blood from PEG₄-acid-Tio AuNP mice (left) and PEG₄OH-Tio AuNP mice (right) expressed as a ratio of RBC:WBC counts. For the saline group and 10% PEG₄-acid, there is no significant change in the ratio, but at 4 weeks post-injection for the 60 and 75% groups, there is an increase in RBC count. There are no changes for either percent place exchange of PEG₄OH, suggesting that the more neutral PEG₄OH is more tolerable in higher concentrations than PEG₄-acid. Reproduced from Reference 20.

GS AuNP Mouse Studies

Monodentate GS AuNPs were seen to exhibit a circulation time of at least 8 weeks with no renal toxicity, which is promising for *in vivo* applications. The first study using monodentate nanoparticles was executed using the same timeline as previous PEG studies: blood and urine collection at baseline, 30 min, 1 hr, 4 hr, 8 hr, 24 hr, 2 wk, 4 wk post-injection, and postmortem organ harvest at 4 weeks. Within 30 min of injection, the blood was clear of nanoparticle, and the urine was clear within 1 hr. At 4 wk post-injection, there was a spike in gold concentration in the blood and urine, but by the time of analysis, the mice had already been euthanized so it was impossible to further investigate. The 20 mg/kg group had a higher concentration in the organs selected for their roles in filtration and high volume blood flow (spleen, kidney, liver, heart) than the 80 mg/kg group, excluding the liver. This is possibly accounted for by the higher concentration of gold in the urine of the 80 mg/kg mice, showing more clearance of particle than the lower concentration group mice.

A second study was conducted with plans to carry out to 8 weeks to determine how long the spike that occurred at 4 weeks would last. Beginning 3 weeks post-exposure, the availability of gold in the bloodstream appeared to have a roughly biweekly periodicity in which the concentration was high for 2 weeks, low for 2 weeks, and then high again for 2 weeks. The gold concentration in the blood did not rise significantly above baseline until 3 weeks post-injection, at which point it reached 42 ppb for 20 mg/kg and 28 ppb for 80 mg/kg. A maximum of 86 and 33 ppb was reached for 20 and 80 mg/kg, respectively, at 4 weeks post-exposure, but by the 5-week mark both dosage groups had fallen back near the baseline. Another spike in gold concentration in the

blood occurred 7 weeks post-injection giving values of 30 ppb (20 mg/kg) and 32 ppb (80 mg/kg). By the 8-week time-point, the 20 mg/kg group averaged 33 ppb while the 80 mg/kg group had decreased to 14 ppb.

The concentration of gold in the urine exhibited a less well defined periodicity that very roughly corresponds to spikes in the gold concentration in blood. At 24 hours and 2 weeks post-injection, the concentration was elevated in the urine while it was near baseline in the blood. This may be due to particle expulsion from renal tissue if the particles were immediately sequestered to the organs and thus removed from blood circulation. A slight decrease in gold concentration in the urine was observed at 3 weeks, with another small spike at 4 weeks. Once again, the concentration fell slightly over weeks 5 and 6, but reached a maximum of 31 and 46 ppb for 20 and 80 mg/kg at 7 weeks. The concentration again fell to 12 ppb (20 mg/kg) and 14 ppb (80 mg/kg) by 8 weeks post-exposure.

Mice were sacrificed 8 weeks post-injection and organs were excised for gold analysis. The results, corrected for mass difference, show the largest retention of GS AuNPs in the liver, followed by the spleen, then the heart and kidney for the 20 mg/kg dosage group. However, the spleen had a slightly higher concentration of gold than the liver in the 80 mg/kg group. Histology of the kidneys for both studies showed no significant lesions, and thus no toxicity.

The biodistribution data agrees with accounts of free extracellular GSH, which report rapid sequestration to the organs, primarily the kidney for hydrolysis and reassembly in the liver.²⁵ Free GSH has also been observed in the spleen.²⁴ While the GS monolayer is presumed to be responsible for the immediate removal of the GS AuNP

from the blood to the organs, AuNPs with other capping ligands²⁰ have also been shown to accumulate in the organs. These nanoparticles cleared steadily from the body and did not exhibit the periodic spikes in concentration that the GS AuNP did, so while retention in the organs may be a general property of AuNPs, it is clear the protecting ligand also affects the behavior of the particles.

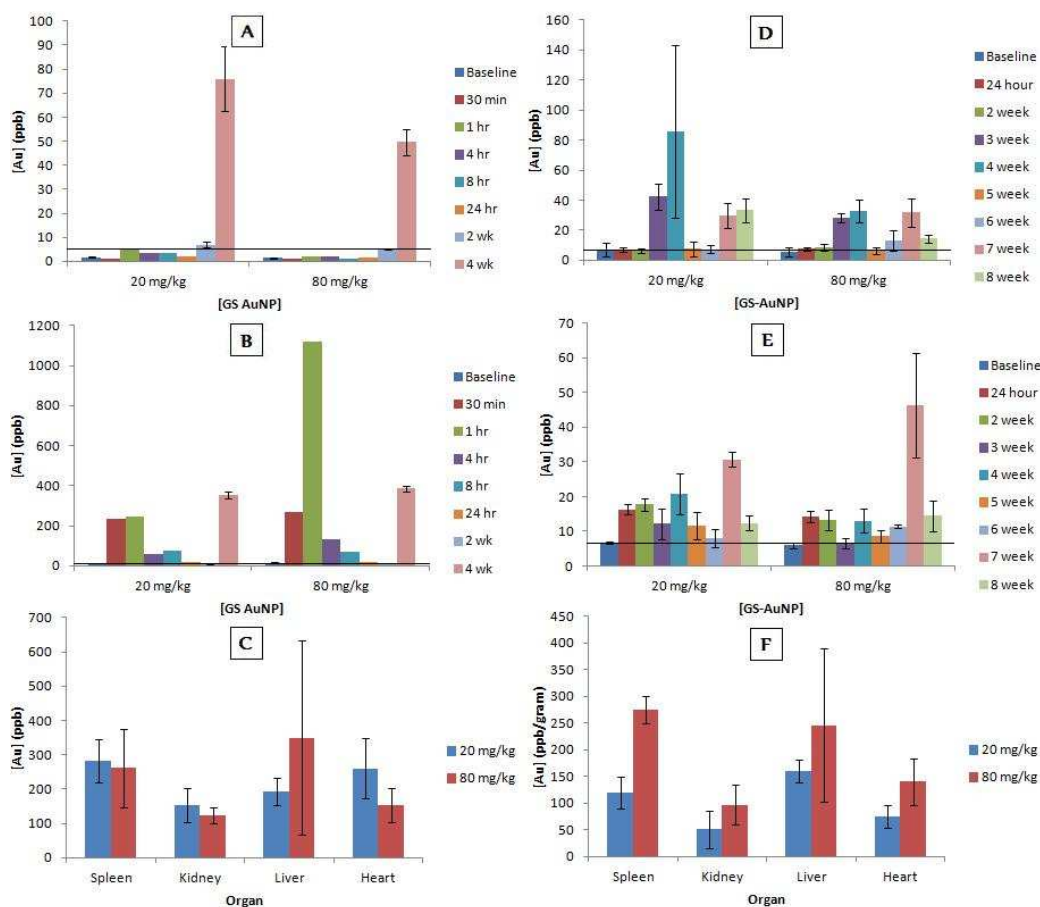


Figure 9. Gold concentration measured using ICP-OES in A) blood, B) urine, and C) organs of mice injected with monodentate GS AuNPs and terminated at 4 weeks post-exposure, and D) blood, E) urine, and F) organs of mice terminated 8 weeks after injection. Samples contained 5 μ L biological fluid or whole organ dissolved in 10 mL 10% aqua regia. AuNPs were immediately removed from the blood and sequestered to the organs, where they were released back into the blood at certain time-points for clearance. For organs obtained 4 weeks post-injection, there is a higher concentration of particles for the 20 mg/kg group, except for in the liver. In the organs collected 8 weeks post-injection, the opposite is seen; the 80 mg/kg group had a higher residence in all organs. Error bars are shown for the organs ($n=5$) and for $n=5$ time-points in the blood and urine, but for the time-points of 30 min, 1 hr, 4 hr, 8 hr, and 24 hr, $n=1$ because NIH bleeding guidelines restrict multiple collections of the necessary blood volume from the same mice within 1 week.

The long circulation time of >8 weeks and non-toxicity make GS AuNPs a good candidate for use as a pharmaceutical scaffold, in this case, for attachment of a peptide epitope mimic. A third study was performed, this time using bidentate GS AuNPs. The concentration groups consisted of a saline group (0 mg/kg), 80 mg/kg, and two more 80 mg/kg groups functionalized with loop or linear PA. Saline and unmodified 80 mg/kg groups were carried out to 8 weeks, while the PA conjugated groups were sacrificed at 4 weeks post-injection because the serum antibody level during the primary response to antigens peaks around 2 weeks, and plateaus for several days to several weeks afterwards.⁴⁰

Bidentate nanoparticles unexpectedly showed a very different clearance profile from monodentate GS AuNPs, as evidenced in Figure 10. At 24 hr post-exposure, there was a very low concentration of no more than 5 ppb in the blood, and no more than 8 ppb in the urine of all three 80 mg/kg groups. This is expected to be the tail of a large spike during which the nanoparticles were largely cleared through the urine. In neither the blood nor urine was there any measurable gold at any other time-point for the duration of the 8 week study. The fast clearance was further evidenced by the overall lower concentration of gold in all measured organs compared to monodentate GS AuNPs.

The biodistribution of the PA functionalized and unfunctionalized GS AuNPs was also different. Unmodified particles were most retained by the liver, followed by the spleen, heart, and then kidney. Linear PA particles had roughly the same concentration in all organs, with slightly less in the heart; the same applies to loop PA, except that there is more than twice as much gold in the kidney than in linear PA and unmodified GS AuNPs. The difference in secondary structure of the loop PA vs. linear somehow causes

more loop PA particles to be caught in the kidneys – perhaps the higher rigidity of structure makes these particles too large to cross the renal threshold. Overall, there is less gold in the analyzed organs of the PA mice, possibly caused by a redirection of nanoparticles to other untested organs because of the difference in the monolayer.

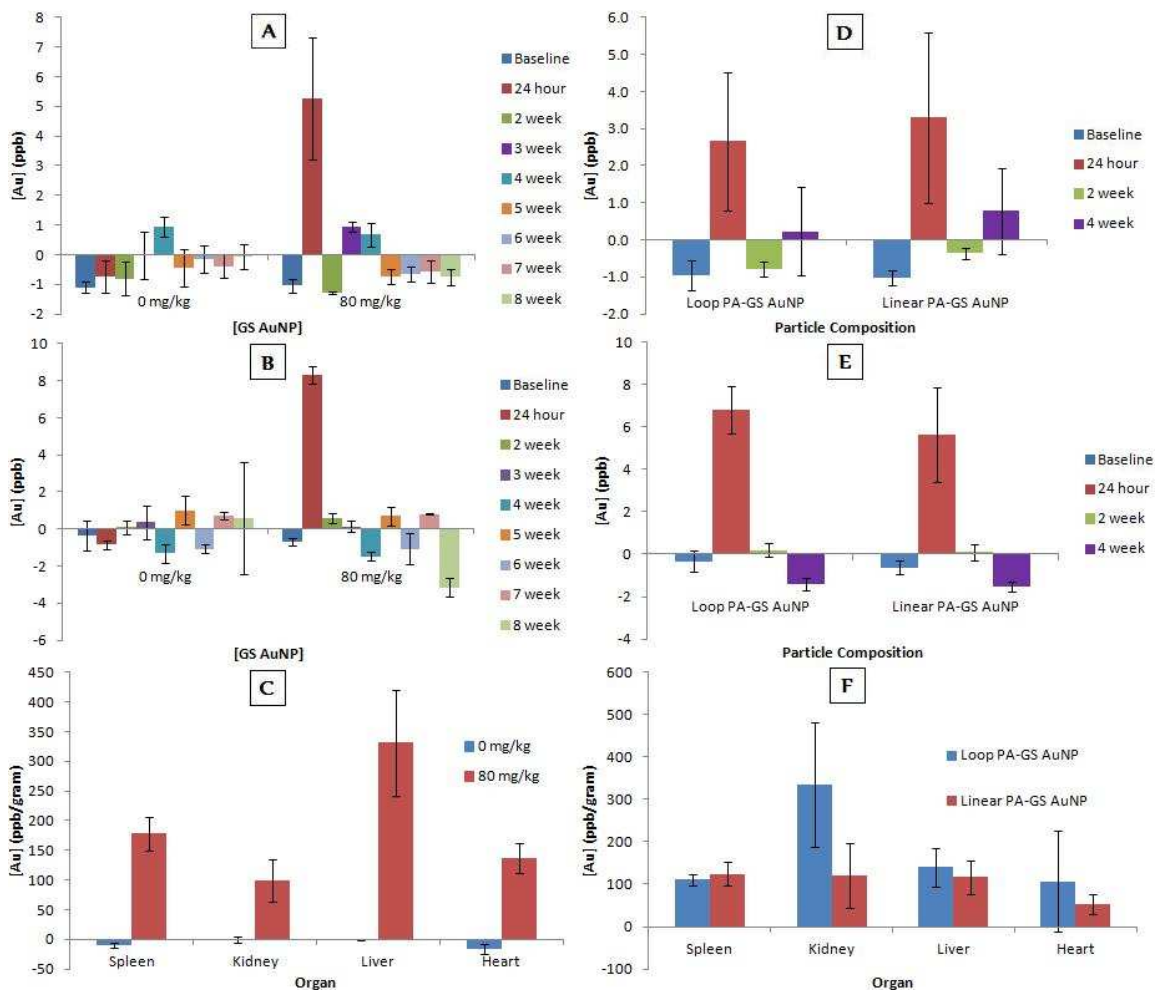


Figure 10. Gold concentration measured using ICP-OES (n=5) in A) blood, B) urine, and C) organs of mice injected with bidentate GS AuNPs and terminated at 8 weeks post-exposure, and D) blood, E) urine, and F) organs of mice inoculated with loop or linear PA functionalized GS AuNPs terminated 4 weeks after injection. Samples contained 5 μ L biological fluid or whole organ dissolved in 10 mL 10% aqua regia. AuNPs were immediately removed from the blood and sequestered to the organs, where they presumably remained for the duration of the study. The biodistribution of unmodified GS AuNPs varied from PA functionalized particles. Loop PA AuNPs accumulated more than twice as much in the kidney than linear PA and unmodified GS AuNPs.

Competitive sandwich ELISA was used to assess antibody production in mice inoculated with GS AuNPs, shown in Figure 11. Blood was pooled from all subjects in each concentration group and four replicates of each were analyzed, with sera diluted 1:20. The first four bars in the chart represent sera of mice injected with loop and linear PA-GS AuNPs, GS AuNPs, and saline. The next bar is for wells containing no serum, giving the highest absorbance because there is no competition for PA binding sites. Sera-containing wells experience a decrease in absorbance because of non-specific binding of serum proteins. Presence of anti-PA antibodies produced by inoculated mice would be marked by a significant decrease in one sera concentration group above the others, but as there is none, it is not likely that such antibodies are present. The remaining three bars represent controls for which no absorbance is expected: no serum and no PA, saline serum with no PA, and GS AuNP serum with no PA.

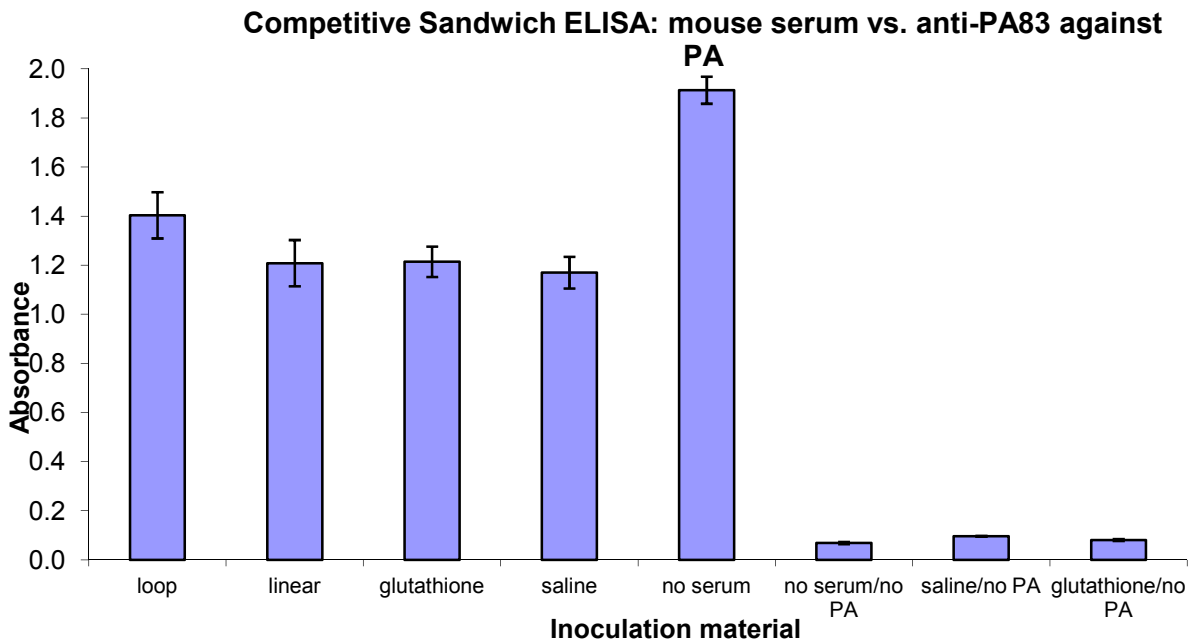


Figure 11. Absorbances measured in ELISA (n=4) for controls and in sera of mice injected with loop and linear PA-GS AuNPs, GS AuNPs, and saline. An immune response would be indicated by a significantly lower absorbance in one serum group than the others, but as there is no real difference, there is no evidence of anti-PA antibodies the in sera of any inoculated mice.

TioEG MPC Mouse Studies

ICP-OES analysis of blood, urine, and organs from mice injected with TioEG MPCs is shown below in Figure 12. Most likely due to their subnanometer size, MPCs were rapidly cleared from the blood and urine within 24 hours. A large amount of particle was eliminated by filtration evidenced by the high concentration in the urine, reaching a maximum of ~1500-2000 ppb in the higher concentration groups at 1 hour post-injection. Heavy retention was observed in the spleen, kidney, liver, lungs, and heart. As was noted for loop PA-GS AuNPs, loop PA-TioEG MPCs also accumulated in the kidneys at a higher rate than the other types of particles. Chen and coworkers⁴¹ report the positive correlation between the concentration of immunogenic nanoparticle in the spleen and the specific antibody response detected. PA-TioEG MPCs accumulated in ~3.5x higher concentrations in the spleen than PA-GS AuNPs, increasing the possibility of detecting anti-PA antibodies.

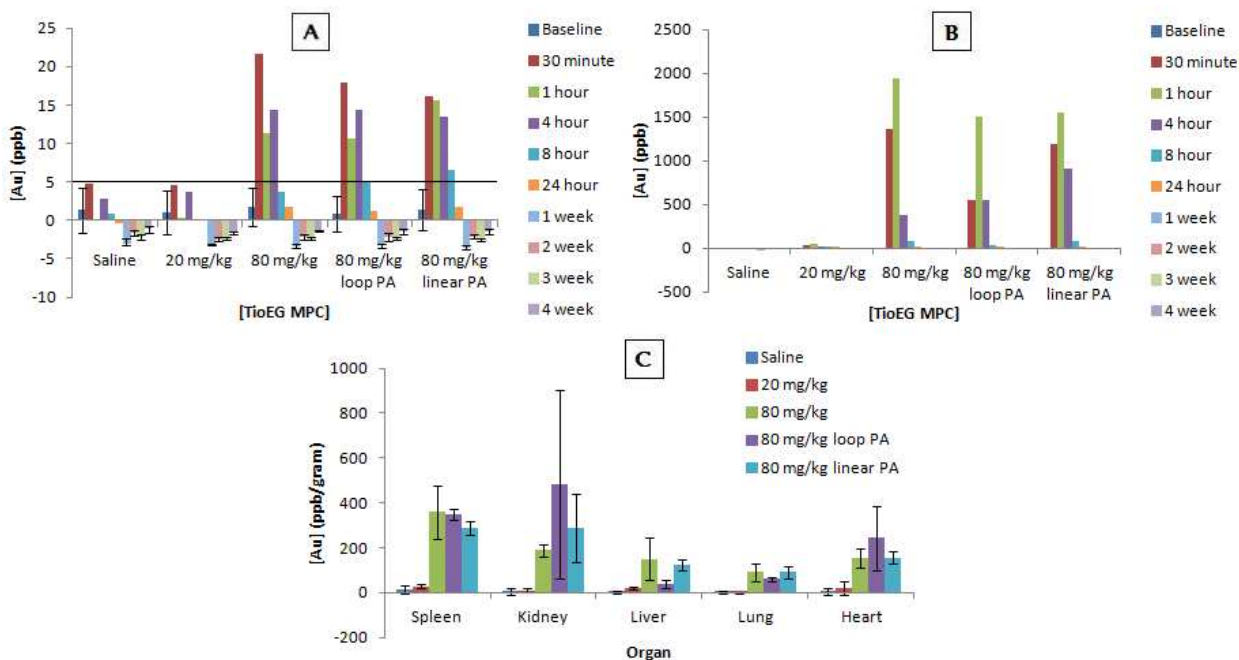


Figure 12. Gold concentration measured using ICP-OES in A) blood, B) urine, and C) organs of mice injected with TioEG MPCs and MPCs conjugated with loop and linear PA. Samples contained 5 μ L biological fluid or whole organ dissolved in 10 mL 10% aqua regia. All MPCs were essentially cleared from the blood and urine within 24 hours and were retained in the organs. Loop PA-TioEG MPCs were retained more heavily in the kidney than other particle types. Error bars are shown for the organs (n=5) and for n=5 time-points in the blood and urine, but for the time-points of 30 min, 1 hr, 4 hr, 8 hr, and 24 hr, n=1 because NIH bleeding guidelines restrict multiple collections of the necessary blood volume from the same mice within 1 week.

For a normal healthy mouse, RBC counts range from $6.36\text{-}9.42 \times 10^6$ cells/ μ L, and WBC counts range from $1.8\text{-}10.7 \times 10^3$ cells/ μ L. All measurements obtained fell within these normal ranges. The WBC count is shown below in Figure 13 for each MPC type. No immune response is observed as the natural fluctuations in WBC count are not outside the tolerable range and no significant trend is noted. The slight downward trend seen in the loop PA MPCs is attributed to natural drift in WBC count, not an effect of nanoparticle inoculation.

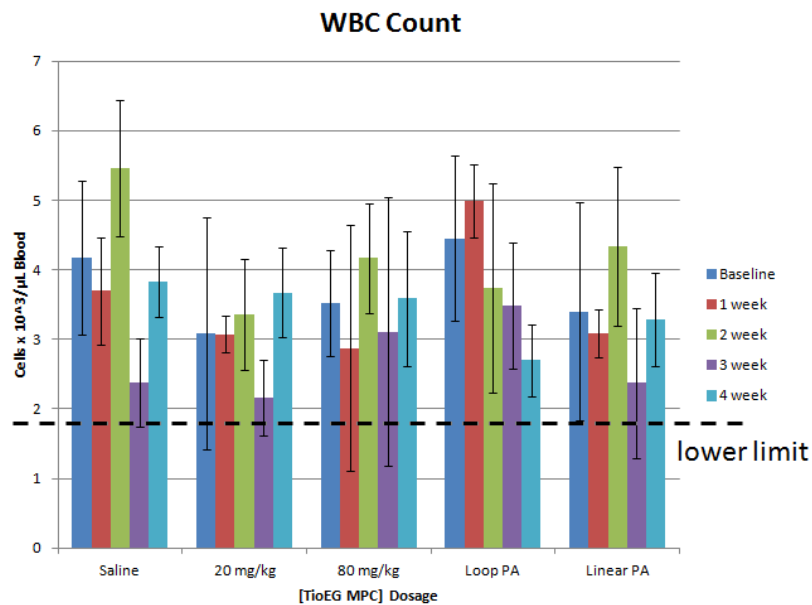


Figure 13. WBC counts obtained by CBC at baseline and 1, 2, 3, and 4 weeks post-exposure. The normal WBC range for mice is $1.8-10.7 \times 10^3$ cells/ μL ; the lower limit is shown as a dotted line on the figure. No immune response is indicated because the natural fluctuations of WBC counts did not fall outside of acceptable limits and no trend is observed, the exception being the slight downward trend in the loop PA-TioEG MPC mice, which is not significant.

The calibration curve for a control ELISA is shown in Figure 14. The volume of HRP-labeled antibody added to each well was held constant while varied volumes of unlabeled antibody 110 were added to each control well. As the result of competition for binding sites on the bound PA protein, the absorbance decreased linearly as increasing amounts of unlabeled antibody were added to the labeled antibody.

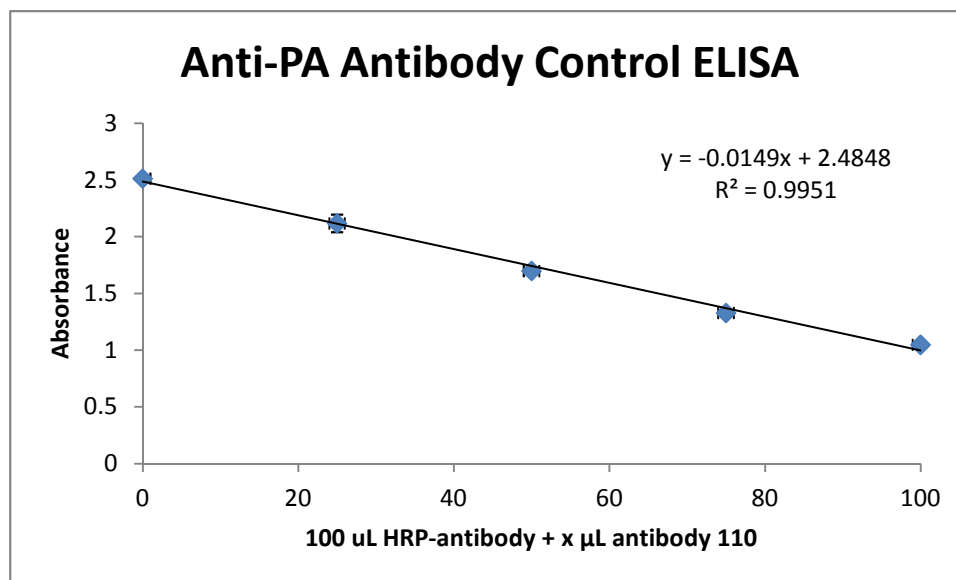


Figure 14. Calibration curve for control ELISA (n=2). A constant amount of HRP-antibody was mixed with increasing amounts of unlabeled antibody 110, resulting in a linear decrease in absorbance as unlabeled antibody competed with labeled antibody for binding sites on PA.

Using a slightly modified version of the competitive sandwich ELISA procedure used for testing GS AuNPs, anti-PA antibodies were detected in the sera of mice inoculated with loop PA-TioEG MPCs. The PA standard used in these experiments was obtained from List Biological Labs, Inc. and used at 1000 ng/mL concentrations. In Figure 15, the highest absorbance is observed in the control wells containing no serum, as there were no serum proteins or other antibodies to block or compete for PA binding sites. As before in the GS AuNP studies, blood was pooled from all subjects in each concentration group and four replicates of each serum group were used. The first four bars on the graph show absorbances from wells containing 1:50 diluted serum of mice inoculated with saline, TioEG MPCs, loop PA-TioEG MPCs, and linear PA-TioEG MPCs. All absorbances were much lower than the no serum control wells because of non-specific binding of serum proteins, so the presence of anti-PA antibodies would be evidenced in serum wells that had significantly lower absorbances than the saline serum.

Conventionally, data with a p value < 0.05 is considered to be statistically significant compared to the baseline (saline serum). While TioEG MPC serum had no significant difference from the saline group, the loop PA-TioEG MPC group was significantly different at a 99% confidence interval (p=0.0093). The linear PA-TioEG MPC group was also different from saline, but only at a 90% confidence interval (p=0.0738). This would indicate that both groups of mice receiving loop and linear PA were able to produce anti-PA antibodies, though the loop PA was the more effective biological mimic. The last bar in the graph represents another control having no PA and no serum.

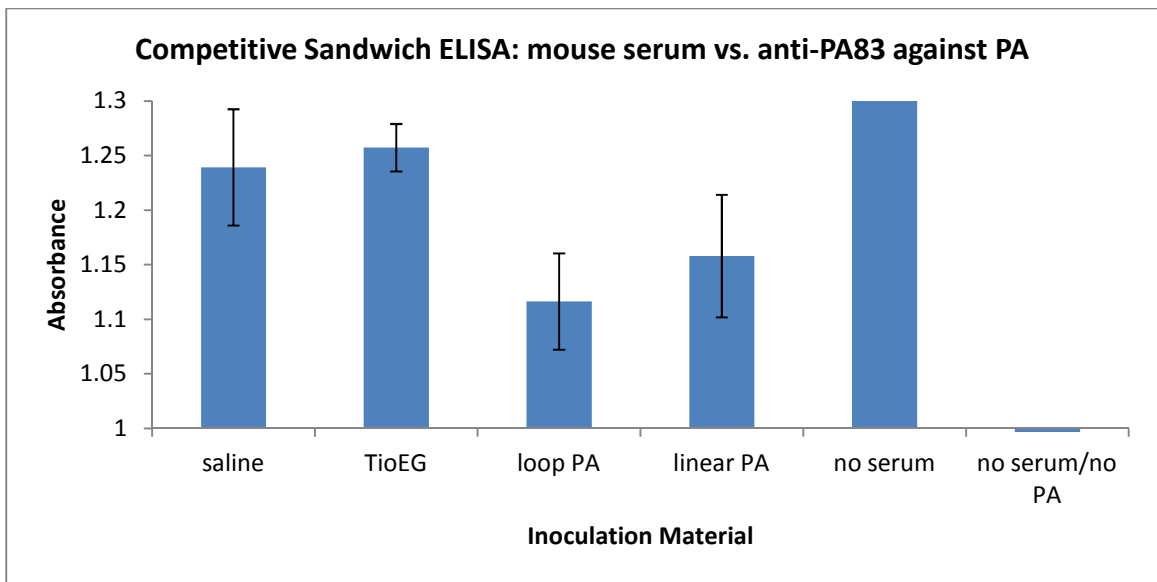


Figure 15. Absorbances measured in ELISA for controls and in sera of mice injected with saline, TioEG MPCs, loop and linear PA-TioEG MPCs (n=4). An immune response would be indicated by a significant difference in one serum group from the saline group, as seen in the loop PA MPCs (p=0.0093, 99% CI) and less significantly (90% CI) in the linear PA MPCs (p=0.0738). This indicates the presence of anti-PA antibodies in sera of mice inoculated with loop and linear PA MPCs. There is no significant difference between the saline group and the TioEG MPC group. The absorbance for the no serum control was measured at 2.51 ± 0.0014 and the no serum/no PA control had an absorbance of 0.0048 ± 0.0059 .

CHAPTER IV

CONCLUSIONS AND FUTURE WORK

Conclusions

The toxicity associated with Tio AuNPs *in vivo* has been shown to be eliminated with PEG-ylation, but high concentrations of PEG invoke an immune response and possibly the formation of anti-PEG antibodies.¹⁹ To be an effective scaffold, Tio AuNPs must be PEG-ylated with a ligand that will allow them to stay in circulation long enough for the body to create antibodies to the target epitope without causing an immune response to the PEG itself. Longer chain lengths allow for longer circulation times, so PEG₄OH and PEG₄-acid may not be the ideal ligand choice since both were mostly cleared within 24 hours after injection.²⁰ Additionally, alcohol terminated PEG thiols seem to be a better choice than carboxylic acid terminated PEG ligands because a higher exchange rate was tolerated without a change in blood cell count.

GS AuNPs also proved to be non-toxic and have no adverse effects on the mice. After rapid removal from the bloodstream to the organs, it appeared that monodentate GS AuNPs were expelled from the organs roughly every two weeks beginning three weeks post-injection while bidentate particles were presumed to have cleared rapidly. Though the long circulation time of monodentate particles seemed promising for utilization as a scaffold, mice inoculated with bidentate particles functionalized with PA did not produce detectable anti-PA antibodies. If the protecting layer of GS was undergoing biodegradation in the organs, this may have destabilized the nanoparticles to the point

that they were destroyed, releasing PA from their surface and preventing proper presentation of the epitope, so no antibodies could form.

Of the nanoparticles studied *in vivo* here, we conclude that TioEG MPCs make the best candidate for use in creating an adjuvant suitable for presenting the conformational peptide epitope of the protective antigen of *B. anthracis*. TioEG MPCs were only in circulation for 24 hr but this combined with their organ residence, particularly the spleen, was sufficient for the mice inoculated with loop, and to a lesser extent linear, PA functionalized MPCs to produce antibodies, as determined by ELISA data.

Future Work

In the future we are interested in studying other epitopes conjugated to gold nanoparticles. Cilengitide is a molecule based on the cyclic peptide motif RGDfV that is selective for α_v integrins, which are important in angiogenesis. Angiogenesis is a common target in cancer treatment as new tumors must become quickly vascularized. We are interested in using a modified Cilengitide containing cyclic and linear RGDfV to functionalize gold nanoparticles for the purpose of imaging lung tumors and emerging metastases with the added side effect of enhanced radiation sensitivity due to absorption by the gold core.

Lung cancer is the most deadly form of cancer with 5-year relative survival rates of only 13.6% for men and 17.5% for women. As radiotherapy plays a central role in treatment of non-small cell lung cancer, a better contrast agent for imaging that could improve radiation sensitivity would be a much needed development. Herold et al. have

shown *in vitro* and *in vivo* proof that gold microspheres introduced to cancer cell lines or injected directly into tumors increased the dosage of X-ray radiation received by >40%.⁴² However these microspheres were unable to target the tumor cells explicitly. Popovtzer et al. showed *in vitro* that gold nanorods conjugated to UM-A9 antibodies specifically bound to head and neck cancers and effectively increased contrast in CT images by 5x compared to untargeted cancer cells and normal cells.⁴³

Our first objective will be to synthesize and characterize gold nanoparticles conjugated to RGDfV peptide in loop and linear form. After that, the efficiency of nanoparticle binding to cancer cell lines *in vitro* will be determined and the successful nanoparticles will be subsequently studied *in vivo* as imaging contrast agents for X-ray radiography and CT imaging.

Acknowledgements

This work was made possible through funding from the NIH (R01 GM 076479).

REFERENCES

- (1) Baillie, L. *Journal of Applied Microbiology* **2001**, *91*, 609-613.
- (2) May, R. J.; Beenhouwer, D. O.; Scharff, M. D. *The Journal of Immunology* **2003**, *171*, 4905-4912.
- (3) De Silva, B. S.; Egodage, K. L.; Wilson, G. S. *Bioconjugate Chemistry* **1999**, *10*, 496-501.
- (4) Rubinchik, E.; Chow, A. W. *Vaccine* **2000**, *18*, 2312-2320.
- (5) Maitta, R. W.; Datta, K.; Lees, A.; Belouski, S. S.; Pirofski, L.-a. *Infection and Immunity* **2004**, *72*, 196-208.
- (6) Gerdon, A. E.; Wright, D. W.; Cliffel, D. E. *Angew Chem Int Edit* **2006**, *45*, 594-598.
- (7) Brust, M.; Walker, M.; Bethell, D.; Schiffrin, D. J.; Whyman, R. *Journal of the Chemical Society, Chemical Communications* **1994**, 801-802.
- (8) Templeton, A. C.; Chen, S.; Gross, S. M.; Murray, R. W. *Langmuir* **1998**, *15*, 66-76.
- (9) Templeton, A. C.; Wuelfing, W. P.; Murray, R. W. *Acc. Chem. Res.* **2000**, *33*, 27-36.
- (10) Whetten, R. L.; Khoury, J. T.; Alvarez, M. M.; Murthy, S.; Vezmar, I.; Wang, Z. L.; Stephens, P. W.; Cleveland, C. L.; Luedtke, W. D.; Landman, U. *Adv. Mater. (Weinheim, Ger.)* **1996**, *8*, 428-433.
- (11) Jadzinsky, P. D.; Calero, G.; Ackerson, C. J.; Bushnell, D. A.; Kornberg, R. D. *Science* **2007**, *318*, 430-433.
- (12) Hostetler, M. J.; Templeton, A. C.; Murray, R. W. *Langmuir* **1999**, *15*, 3782-3789.
- (13) Alexis, F.; Pridgen, E.; Molnar, L. K.; Farokhzad, O. C. *Molecular Pharmaceutics* **2008**, *5*, 505-515.
- (14) Owens III, D. E.; Peppas, N. A. *International Journal of Pharmaceutics* **2006**, *307*, 93-102.
- (15) Moghimi, S. M.; Hunter, A. C.; Murray, J. C. *Pharmacological Reviews* **2001**, *53*, 283-318.
- (16) Chen, Z.; Meng, H.; Xing, G.; Chen, C.; Zhao, Y.; Jia, G.; Wang, T.; Yuan, H.; Ye, C.; Zhao, F.; Chai, Z.; Zhu, C.; Fang, X.; Ma, B.; Wan, L. *Toxicology Letters* **2006**, *163*, 109-120.
- (17) Choi, H. S.; Liu, W.; Misra, P.; Tanaka, E.; Zimmer, J. P.; Ipe, B. I.; Bawendi, M. G.; Frangioni, J. V. *Nat Biotechnol* **2007**, *25*, 1165-1170.
- (18) Moghimi, S. M.; Porter, C. J. H.; Muir, I. S.; Illum, L.; Davis, S. S. *Biochemical and Biophysical Research Communications* **1991**, *177*, 861-866.
- (19) Simpson, C. A.; Huffman, B. J.; Gerdon, A. E.; Cliffel, D. E. *Chemical Research in Toxicology* **2010**.
- (20) Simpson, C. A.; Agrawal, A. C.; Balinski, A.; Harkness, K. M.; Cliffel, D. E. *ACS Nano* **2011**, *5*, 3577-3584.
- (21) Armstrong, J. K.; Leger, R.; Wenby, R. B.; Meiselman, H. J.; Garratty, G.; Fisher, T. C. *Blood* **2003**, *102*, 556A.

- (22) Wu, G.; Fang, Y.-Z.; Yang, S.; Lupton, J. R.; Turner, N. D. *The Journal of Nutrition* **2004**, *134*, 489-492.
- (23) Witschi, A.; Reddy, S.; Stofer, B.; Lauterburg, B. H. *Eur. J. Clin. Pharm.* **1992**, *43*, 667-669.
- (24) Hahn, R.; Wendel, A.; Flohe, L. *Biochemica et Biophysica Acta* **1978**, *539*, 324-337.
- (25) Wendel, A.; Jaeschke, H. *Biochem Pharmacol* **1982**, *31*, 3607-3611.
- (26) Alvarez, M. M.; Khoury, J. T.; Schaaff, T. G.; Shafiqullin, M.; Vezmar, I.; Whetten, R. L. *Chem. Phys. Lett.* **1997**, *266*, 91-98.
- (27) Negishi, Y.; Chaki, N. K.; Shichibu, Y.; Whetten, R. L.; Tsukuda, T. *J. Am. Chem. Soc.* **2007**, *129*, 11322-11323.
- (28) Zhu, M.; Aikens, C. M.; Hendrich, M. P.; Gupta, R.; Qian, H.; Schatz, G. C.; Jin, R. *Journal of the American Chemical Society* **2009**, *131*, 2490-2492.
- (29) Wu, Z.; Suhan, J.; Jin, R. C. *Journal of Materials Chemistry* **2009**, *19*, 622-626.
- (30) *Handbook of Preparative Inorganic Chemistry*; 1st ed.; Brauer, G., Ed.; Academic Press: New York, 1965.
- (31) Balinski, A., Vanderbilt University, 2010.
- (32) Harkness, K. M.; Hixson, B. C.; Fenn, L. S.; Turner, B. N.; Rape, A. C.; Simpson, C. A.; Huffman, B. J.; Okoli, T. C.; McLean, J. A.; Cliffler, D. E. *Analytical Chemistry* **2010**, *82*, 9268-9274.
- (33) Karas, M.; Hillenkamp, F. *Analytical Chemistry* **1988**, *60*, 2299-2301.
- (34) Golde, W. T., Gollobin, P., and Rodriguez, L. L. *Lab Anim* **2005**, *34*, 39-43.
- (35) NIH *Guidelines for Survival Bleeding of Mice and Rats*, 2005.
- (36) Kurien, B. T.; Scofield, R. H. *Lab Anim* **1999**, *33*, 83-86.
- (37) Kohlmann, O.; Steinmetz, W. E.; Mao, X.-A.; Wuelfing, W. P.; Templeton, A. C.; Murray, R. W.; Johnson, C. S. *The Journal of Physical Chemistry B* **2001**, *105*, 8801-8809.
- (38) Nimmala, P. R.; Dass, A. *Journal of the American Chemical Society* **2011**, *133*, 9175-9177.
- (39) Alvarez, M. M.; Khoury, J. T.; Schaaff, T. G.; Shafiqullin, M. N.; Vezmar, I.; Whetten, R. L. *J Phys Chem B* **1997**, *101*, 3706-3712.
- (40) Goldsby, R. A. K., T. J.; Osborne, B. A.; Kuby, J.; 5th ed.; W. H. Freeman & Co.: 2003, p 264.
- (41) Chen, Y.-S.; Hung, Y.-C.; Lin, W.-H.; Huang, G. S. *Nanotechnology* **2010**, *21*, 95101.
- (42) M. Herold, I. J. D., C. C. Stobbe, R. V. Iyer, J. D. Chapman, D. *International Journal of Radiation Biology* **2000**, *76*, 1357-1364.
- (43) Popovtzer, R.; Agrawal, A.; Kotov, N. A.; Popovtzer, A.; Balter, J.; Carey, T. E.; Kopelman, R. *Nano Letters* **2008**, *8*, 4593-4596.